Positron emission profiling : a study of hydrocarbon diffusivity in MFI zeolites

Mol Sieves (2008) 7: 277–328
DOI 10.1007/3829_2007_014

Published online: 2 October 2007

Positron Emission Profiling: a Study of Hydrocarbon Diffusivity in MFI Zeolites

E. J. M. Hensen[1] (✉) · A. M. de Jong[2] · R. A. van Santen[1]

[1]Schuit Institute of Catalysis, Faculty of Chemical Engineering and Chemistry, Eindhoven University of Technology, PO Box 513, 5600MB Eindhoven, The Netherlands
e.j.m.hensen@tue.nl

[2]Accelerator Laboratory, Schuit Institute of Catalysis, Faculty of Technical Physics, Eindhoven University of Technology, PO Box 513, 5600MB Eindhoven, The Netherlands

Abstract Zeolites are of prime importance to the petrochemical industry as catalysts for hydrocarbon conversion. In their molecule-sized micropores, hydrocarbon diffusion plays a pivotal role in the final catalytic performance. Here, we present the results of Positron Emission Profiling experiments with labeled hydrocarbons in zeolites with the MFI morphology. Single-component self-diffusion coefficients of hexanes in silicalite-1 and its acidic counterpart H-ZSM-5 are determined. For the first time, self-diffusion co-

efficients of *n*-pentane and *n*-hexane in mixtures are studied. This shows that Positron Emission Profiling is a powerful technique for in situ investigations of the adsorptive and diffusive properties of hydrocarbons in zeolites. The diffusion of hydrocarbons in medium-pore zeolites is determined by a complex interplay of factors such as the loading, the temperature, the preference for certain pore locations, the interactions with other hydrocarbon molecules of the same type or of other types and the presence of acid protons. In the diffusion of mixtures, pore blockage by one of the components might occur, thus strongly decreasing the diffusivity of the faster diffusing hydrocarbon.

Abbreviations

BGO	Bismuth germanium oxide
c	concentration
c^*	Concentration of labeled molecules
c_0	Concentration
c_{gas}	Concentration in gas phase
c_{max}	Maximum concentration
c_x	Concentration inside zeolite crystals
c_z	Concentration along reactor axis z
$c_{z,0-}$	Concentration just in front of column entrance
$c_{z,0+}$	Concentration just after column entrance
CEM	Controlled evaporator and mixer
CBMC	Configurational bias Monte Carlo
D	Diffusion coefficient
D_0	Maxwell–Stefan diffusion coefficient
D_c	Diffusion coefficient inside zeolite crystals
D_{inf}	Diffusion coefficient at infinite temperature
D_t	Transport diffusion coefficient
D_s	Self-diffusion coefficient
D_s^0	Self-diffusion coefficient at infinite dilution
D_{ax}	Axial diffusion coefficient
D_x	Diffusion coefficient
E_{act}	Activation energy
E_{app}	Apparent activation energy
FID	Flame ionization detector
FR	Frequency response
GC	Gas chromatograph
Grav.	Gravimetric
H-ZSM-5	Zeolite structure; cf. [1]
$\overrightarrow{J}$	Flux due to transport diffusion
J	Flux due to transport diffusion in one direction
J_i^*	Flux due to transport diffusion of labeled molecule i
K_a	Adsorption equilibrium constant
K_{ads}	Adsorption equilibrium constant
k_a	Rate constant for adsorption
k_d	Rate constant for desorption
L	Onsager coefficient
LSO	Lutetium oxyorthosilicate

M	Molar mass
MD	Molecular dynamics
MFI	Zeolite structure; cf. [1]
MS	Mass spectrometer
molec.	Molecule(s)
N_c	Mass flux through the boundary of the zeolite crystals
Na-Y	Zeolite structure; cf. [1]
ODE	Ordinary differential equation
p	Partial pressure
PEP	Positron emission profiling
PEPT	Positron emission particle tracking
PET	Positron emission tomography
PFG NMR	Pulsed-field gradient nuclear magnetic resonance
Ps	Positronium
q	Concentration of species adsorbed in pores
R_c	Radius of zeolite crystals
R_g	Ideal gas constant
SEM	Scanning electron microscopy
SCR	Selective catalytic reduction
SCM	Single crystal membrane
t	time
T	Temperature
T_{max}	Maximum kinetic energy of positrons
TAP	Temporal analysis of products
TEOM	tapered element oscillating mass balance
TEX-PEP	tracer-exchange positron emission profiling
uc	unit cell
x	Spatial coordinate
Y	Zeolite structure; cf. [1]
ZLC	Zero length column
z	Coordinate along the reactor axis

Symbols

β	Elementary particle
β^+	Positron
β^-	electron
Γ	Thermodynamic correction factor
ε	Bed porosity
ε_x	Porosity of the zeolite crystals
μ	Chemical potential
μ^0	Chemical potential at standard conditions
Φ_s	Number of collisions between molecules and surface
Θ	Coverage inside the pores of the zeolite
v_{int}	Interstitial velocity
v_{sup}	Superficial velocity

1 Introduction

1.1 Zeolites in Catalysis

Since the 1960s, zeolites have been applied in an increasing number of catalytic processes. Zeolites are crystalline microporous materials close to sand in composition, but with a much wider diversity in structures mainly due to their porous nature and possibilities for functionalization. The silicon-containing oxygen tetrahedra are the basic building blocks to all kinds of structures with pores and cavities of varying dimensions. Up to now, 136 different structures have been reported [1], of which about 40 are naturally occurring. These materials look like sponges, but with a very regular structure and pore sizes, which are typically of molecular dimensions. The topologies of two important medium-pore zeolites are depicted in Fig. 1. The regularly shaped channels in these zeolites can be clearly seen. The different zeolites differ in pore diameter, pore shape and the way these pores are interconnected. Zeolite mordenite has a one-dimensional pore system consisting of channels with a diameter of about 7 Å, while the pores of silicalite-1 form a three-dimensional network of interconnected straight and zigzag channels (shown schematically in Fig. 2) with diameters of about 5.5 Å. While a material like silicalite-1 is neutral and does not contain acid protons, substitution of tetravalent Si by trivalent cations such as Al^{3+} renders these materials Brønsted acidic. As these acid sites are mainly located in the molecularly-

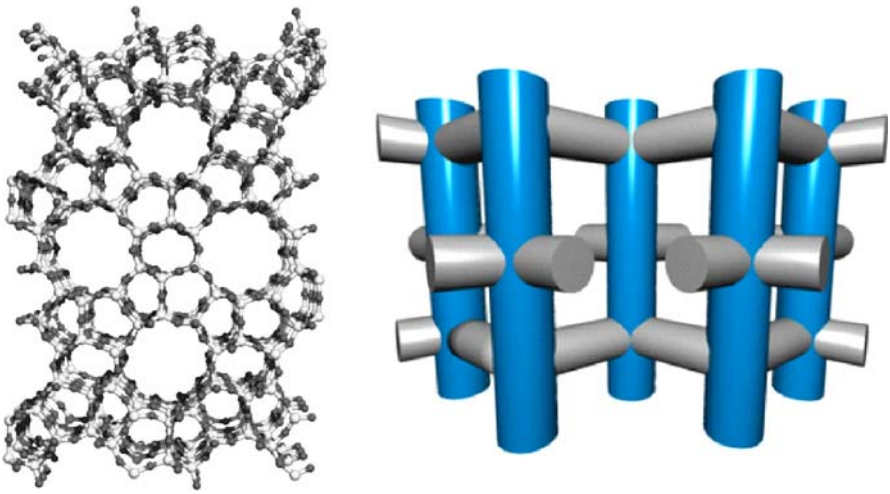

Fig. 1 The structure of the medium-pore zeolite silicalite-1 (*left*) and a schematic representation of the pore system which consists of straight and zigzag channels

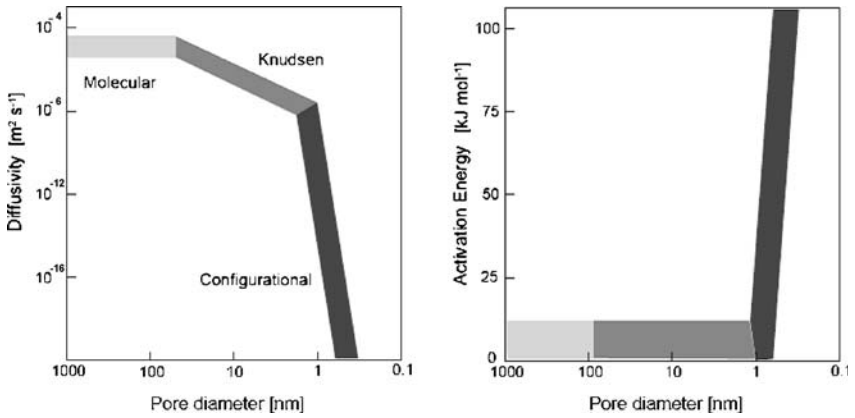

Fig. 2 Effect of pore size on the diffusivity and activation energy of diffusion (taken from Post [7, 8])

sized pore systems, the selectivity of the transformation of molecules such as hydrocarbons can be influenced to a great extent. Different types of selectivity are distinguished, including reactant and product selectivity referring to the sieving properties of the zeolites towards adsorption of reactants and desorption of products and transition-state selectivity referring to the zeolite's pore system to provide limitations to certain transition states. Furthermore, these materials can also act as a support for other catalytic materials (e.g., platinum or palladium), and in this way bifunctional catalysts can be obtained combining acid cracking and hydrogenation-dehydrogenation functionalities.

Among the most important applications of zeolites is the use of these materials to catalyze the conversion of crude oil to more useful products like gasoline, kerosene and other smaller hydrocarbons. A number of different reactions are involved in this conversion, like hydrocracking, hydroisomerization, aromatization and dehydrogenation of cyclohexanes. Catalytic cracking is one of the largest applications of catalysts, with a worldwide production of more than 500 million tons per year. One example of the processes nowadays performed in oil refineries is the so-called Hysomer process, developed by Shell for the hydroisomerization of linear alkanes to branched ones. This process makes use of platinum-loaded acidic mordenite, and is a typical example in which the zeolite acts as a bifunctional catalyst. Pt catalyzes the hydrogenation and dehydrogenation of alkanes, while the acid sites of the zeolites catalyze the conversion of linear alkenes to branched ones. This process is especially useful as it can increase the octane number of the products.

Clearly, the catalytically active sites are not directly accessible to the reacting molecules. The catalytic cycle for zeolite-catalyzed reactions generally encompasses several steps including reactant adsorption, diffusion to the active sites, product formation, diffusion to the surface and product desorption. Because the pores of zeolites have dimensions close to those of the adsorbing

and produced hydrocarbon molecules, the diffusion process is of profound influence on the overall process.

1.2 Diffusion

1.2.1 Introduction

Diffusion in liquids, gases and solids has been studied for more than a century now [2]. The discovery of Brownian motion, which is closely related to diffusion, and the subsequent search for explaining this behavior significantly contributed to the acceptance of the atomic view of matter and kinetic theory of gases and liquids. Diffusion is caused by the thermal motion and subsequent collisions of molecules. Two types of diffusion can be distinguished: transport diffusion resulting from a concentration gradient, and self-diffusion which takes place in a system at equilibrium. The flux due to transport diffusion can be described using Fick's first law of diffusion:

$$\vec{J} = -D \cdot \nabla c \tag{1}$$

in which D is the diffusion constant and c the concentration. Self-diffusion is usually expressed in terms of a self-diffusion constant D_s. In the specific case of tracer diffusion, in which labeled molecules mix with unlabeled molecules with the same chemical properties, the transport and self-diffusivity are identical. Usually, however, although transport and self-diffusion generally occur by essentially the same microscopic principle, the coefficients for transport and self-diffusion are not equal.

Diffusion in zeolites differs from ordinary diffusion in the sense that the molecules have to move through channels of molecular dimensions. As a result, there is a constant interaction between the diffusing molecules and the zeolite framework, and the molecular motion is, thus, also strongly influenced by the exact size and shape of these channels next to parameters such as temperature and concentration. Whereas in the case of gases and liquids the behavior and exact value of the diffusivity can be calculated with relative ease, the exact values of these are much harder to predict for zeolites. The interactions between molecules and the pore wall for example lead to large differences in the diffusivities of different alkane isomers, because bulkier branched isomers have a much larger interaction with the zeolite framework. A special type of diffusion can be observed in one-dimensional zeolites, called *single-file* diffusion. This type of diffusion results from the fact that some types of molecules are unable to pass each other in the narrow pores of the zeolites, leading to a significant reduction of the mobility in these systems. Clearly, these effects are not present in pure liquids and gases.

From an industrial point of view, it is important to be able to predict and describe the mass transfer through the packed-bed reactors used in the chemical industries. A better understanding of this phenomenon will aid in the optimization and development of industrial applications of these materials in separation and catalytic processes. For this purpose, the transport diffusivities are needed. A number of different experimental techniques are nowadays available for determining these values [3]. No reliable theory exists that can easily predict the diffusivity for different components in different zeolites, as it is often hard to relate these values to the underlying microscopic mechanisms [4, 5]. Furthermore, large discrepancies often exist between values obtained from different techniques, and performing these experiments is often not straightforward. It would, thus, be advantageous to have a good understanding of what can happen inside these zeolites, and what kind of influence this will have on a reactor scale.

From a fundamental point of view, the study of diffusion is also interesting as the interactions between molecules and the zeolite can lead to all kinds of unexpected behavior. The dependencies on, for example, the concentration of the diffusing molecules are expected to be completely different, as also the topology of the zeolite pore network plays an important role in this behavior. The diffusion of mixtures of different molecules is also less straightforward. This kind of effects can be readily studied using zeolites, as in a sense, due to their regular structure, they can act as models for more complicated systems like for example amorphous materials. Furthermore, a thorough understanding of the underlying microscopic mechanisms involved will aid in understanding the interaction between transport properties and the reactivity in these materials.

Diffusion of molecules through the pores of a zeolite crystal differs greatly from gaseous diffusion. In gases the diffusion is controlled by the interactions (or collisions) between the different molecules due to their thermal motion. As gases and liquids form an isotropic medium, different properties like the average collision rate, the collision rate and the mean free path can be easily calculated using kinetic theory, based on the laws of classical mechanics [6]. More sophisticated theories, which also account for intermolecular interactions, vibration and rotation of the molecules, and quantum effects are nowadays available and are quite capable of describing the behavior of a variety of systems.

The diffusion of molecules in pores can be classified in a number of different regimes depending on the pore diameter (Fig. 2). For large pore diameters of the order of 1 μm or larger, usually called macropores, collisions between the molecules occurs much more frequently than collisions with the wall, and molecular diffusion is the dominant mechanism. Typically, the diffusion constants of gases are around 10^{-5} m^2 s^{-1}. As the size of the pores decreases, the number of collisions with the wall increases until the diffusion length finally becomes smaller than the mean free path (the average distance traveled

by a molecule between two collisions) of the gas molecules. At this point, Knudsen diffusion takes over, and the mobility starts to depend on the dimensions of the pore [9]. At even smaller pore sizes, in the range of 20 Å and smaller when the pore diameter becomes comparable to the size of the molecules, these will continuously feel the interaction with the walls. Diffusion in the micropores of a zeolite usually takes place in this regime, and is called *configurational* diffusion [10]. The mechanism by which the molecules move through the pores in the configurational regime is comparable to that of surface diffusion of adsorbed molecules on a surface. Due to the small distance between the molecules and the pore wall, the molecules are more or less physically bonded to it. The diffusivity in this regime will depend strongly on the pore diameter, the structure of the pore wall, the interactions between the surface atoms and the diffusing molecules, the shape of the diffusing molecules and the way the channels are connected. As a result, it is very difficult to derive generalized equations relating the aforementioned properties to the diffusion coefficient one finds for these systems. The values of these coefficients, furthermore, span an enormous range from 10^{-8} to as low as 10^{-20} m^2 s^{-1} [4]. Compared to the gas phase, the diffusivity of the molecules inside the zeolite channels is thus greatly reduced and a much stronger temperature dependence is often observed. The fact that the particles have to move through the pore network also introduces correlation effects, which may also greatly enhance the concentration dependence.

1.2.2 Self-Diffusion vs. Transport Diffusion

The foundations of the theory of diffusion were laid by Fick in the 19th century. In one dimension, the flow of a certain species can be related to the gradient of the concentration according to Fick's first law [11]

$$J = - D_t \left(\frac{\partial c}{\partial x} \right) , \tag{2}$$

in which c is the concentration, x is the spatial coordinate, and D_t is the (transport) diffusion coefficient. The diffusion coefficient is, thus, defined as a proportionality constant between the rate of flow and the concentration gradient. Although the above equation is a convenient starting point, it does not reflect the true driving force of diffusion. As diffusion is nothing more than the macroscopic manifestation of the tendency of a system to approach equilibrium, the driving force should be the gradient of the chemical potential μ. Using irreversible thermodynamics, one can derive the Onsager relation:

$$J = - L \left(\frac{\partial \mu}{\partial x} \right) \tag{3}$$

in which L is the phenomenological Onsager coefficient. This equation indeed explicitly identifies the cause for diffusive flow, and will prove to be useful when trying to relate the transport diffusion to self-diffusion.

The pioneering work on zeolitic diffusion, performed by Barrer and Jost [12], was based on the application of Fick's equation. Assuming a concentration-independent diffusion constant, one can transform Eq. 2 into a diffusion equation known as Fick's second law:

$$\frac{\partial c}{\partial t} = - D_{\mathrm{t}} \left(\frac{\partial^2 c}{\partial x^2} \right) . \tag{4}$$

This equation gives the change of concentration in a finite volume element with time. In the approach of Barrer and Jost, the diffusivity is assumed to be isotropic throughout the crystal, as D_{t} is independent of the direction in which the particles diffuse. Assuming spherical particles, Fick's second law can be readily solved in radial coordinates. As a result, all information about the exact shape and connectivity of the pore structure is lost, and only reflected by the value of the diffusion constant.

While for the transport diffusion a gradient in the chemical potential is necessary, self-diffusion is an equilibrium process. This type of diffusion can be monitored by labeling some of the molecules inside the zeolite pores and following how the labeled and unlabeled molecules are mixed. Equation 2 can again be used to describe the flow of the labeled components:

$$J_{\mathrm{i}}^{*} = - D_{\mathrm{s}} \left. \frac{\partial c^{*}}{\partial x} \right|_{c=cons\tan t} \tag{5}$$

in which the asterisk refers to the labeled component, and in this case D_{s} is the self-diffusion constant. Alternatively, the self-diffusion constant can be related to a microscopic quantity called the mean-square displacement, as was shown by Einstein in his study on Brownian motion [13] which is of particular value for evaluation of diffusion coefficient by theoretical methods.

1.2.3 The Darken Relation

As noted earlier, the driving force of diffusion is the gradient of the chemical potential. The chemical potential can be related to the concentration by considering the equilibrium vapor phase:

$$\mu = \mu^{0} + R_{\mathrm{g}} T \ln p , \tag{6}$$

in which p is the partial pressure of the component. Using this equation yields the so-called *Darken equation* – although Darken was not the first to derive it (see in this connection [14]) – which relates the two constants D_{t} and L to

each other:

$$D_t = R_g T L \left(\frac{\partial \ln p}{\partial \ln c} \right) = D_0 \left(\frac{\partial \ln p}{\partial \ln c} \right) = D_0 \Gamma \,. \tag{7}$$

D_0 is generally referred to as the *corrected* or *Maxwell–Stefan* diffusivity, and Γ is called the thermodynamic correction factor, which corrects for the non-linearity between the pressure and the concentration of the adsorbate. Often, the corrected diffusivity is used in experimental studies where the transport diffusion is measured. Although D_0 can still depend on the concentration, in systems near the saturation limit or in the low concentration (Henry's law) regime this dependence has been experimentally shown to be quite small, and the use of the corrected diffusivity helps in directly comparing experimental results under different conditions [3].

A similar expression as Eq. 7 is also used to relate the transport and self-diffusion to each other:

$$D_t(q) = D_s(0) \left(\frac{\partial \ln p}{\partial \ln q} \right) \,, \tag{8}$$

in which q is the concentration of the species adsorbed in the pores. This equation implies that the self- and transport diffusivity coincide at low concentrations. Although the derivation of this relation is rather straightforward [3], the assumption is made that the diffusion process in both completely different experimental situations can be described in a similar fashion. In general this does not have to be the case and deviations from the above expression can be expected [15]. Recently, Paschek and Krishna [14] have suggested that Eq. 7 can indeed be used to relate the transport diffusivity to the Maxwell–Stefan or corrected diffusivity, but that an extra relation is needed to link the corrected and self-diffusivity:

$$D_s = \frac{D_0}{1 + \Theta} \,, \tag{9}$$

in which Θ is the coverage inside the pores of the zeolite.

1.2.4 Factors Influencing Diffusivity

Adsorbate Concentration

In zeolites, the diffusivity of the adsorbates can be strongly dependent on the concentration. As the diffusion of molecules in zeolites takes place in channels where it is difficult or impossible to pass each other, encounters between different molecules will have a much more pronounced influence on the mobility. Barrer [16] explained the concentration dependence of the diffusivity in zeolites using a simple jump model. Assuming that the particle has an elementary diffusion rate D_s^0 at infinite dilution to move from one site to another,

we find that the diffusivity will be proportional to the chance that a neighboring site is empty:

$$D_s(\Theta) = D_s^0(1 - \Theta) . \tag{10}$$

This equation makes use of the fact that, in the mean-field approximation, the average coverage of a site will be equal to Θ. That the actual situation can be rather more complicated has been demonstrated by a number of authors [17–19], who have shown that correlation effects can have a strong impact on the dependence of the diffusivity.

According to Kärger and Pfeifer [20], five different types of concentration dependence of the self-diffusivity (observed with NMR measurements) can be observed, as shown in Fig. 3. These different dependencies can be attributed to differences in the interactions between the framework atoms and the diffusing molecules, like for example interactions with different cations in the zeolite, or the presence of strong and weak adsorption sites. In addition the pore topology can also have a significant influence on the diffusivity, as was shown by Coppens et al. [19]. This is mainly due to the stronger correlations present in systems with lower connectivity. As a result, there is an increased chance that a molecule will move back into its previous location because the chance of finding an empty space at this location is larger. Hence, a larger decrease in mobility with increasing pore loading is observed [3]. The prediction of the concentration dependence for different systems, how-

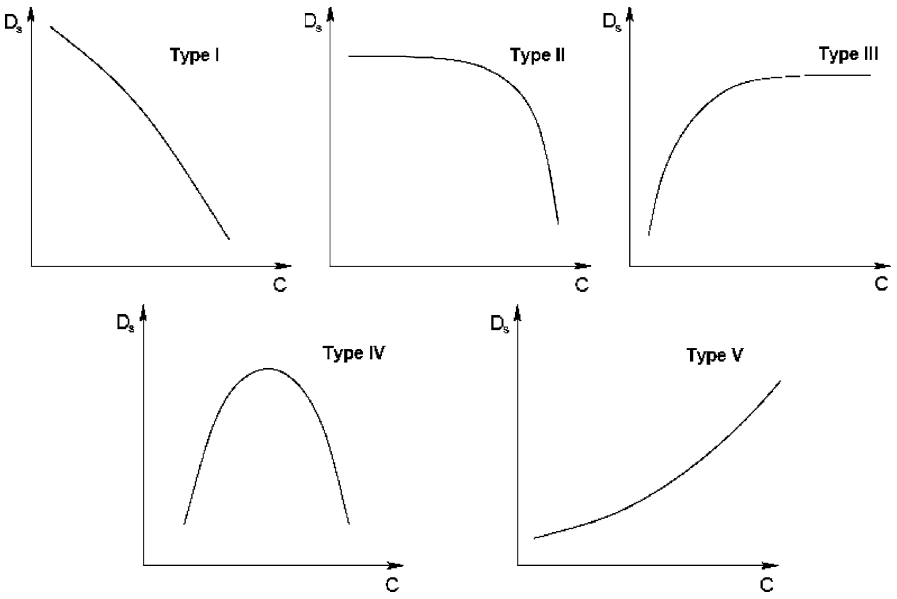

Fig. 3 Types of concentration dependence of the intracrystalline self-diffusion coefficient [20]

ever, remains difficult, and further investigations on this dependence remain of interest.

Temperature

As the molecules are continuously moving in the force field of the zeolite channels, the diffusion process can be described as an activated process, and the temperature dependence can accordingly be described by an Arrhenius-type equation [21]

$$D(T) = D_{\text{inf}} \cdot \exp\left(-\frac{E_{\text{act}}}{R_{\text{g}}T}\right), \tag{11}$$

with D_{inf} the diffusivity at infinite temperature, and E_{act} the activation energy of diffusion. This dependency is usually explained by assuming that diffusion takes place via a sequence of activated hops [22]. The pre-exponential term D_{inf} is related to the elementary rate at which particles attempt to hop to a neighboring adsorption site, while the exponential expresses the chance that the particles are able to overcome the free energy barrier, E_{act}, between these sites. Although this is an oversimplified picture of the true diffusion process, many experimental and theoretical studies have shown that it is capable of accurately describing the temperature dependence in these systems.

Experimentally, the activation energy can thus be determined by measuring the diffusivity at different temperatures. Some care should, however, be taken when interpreting these results. As the concentration of molecules inside the zeolite also depends on the temperature and measurements are often performed at finite loadings, the combined effect of temperature and loading dependence is measured. With increasing temperature, the loading of the zeolite crystals usually decreases. Assuming a type I concentration dependence (cf. [20] and Fig. 3), in addition to the increased mobility of the molecules due to the higher temperatures, we find that this can also lead to an increase of the diffusion rate. As a result, the measured activation energy can in this case be much higher than the real activation energy, and this value will also depend on the gas-phase pressure at which the measurements are performed. This effect has recently been demonstrated for 3-methylpentane in silicalite-1 [23], but the exact influence of the concentration dependence of course depends on the concentration dependence of the system. Ways to circumvent this problem are by measuring at very low coverages, or choosing experimental conditions in such a way that the concentration inside the zeolite remains constant. For systems with a moderate dependence of the diffusivity on the concentration the effect might be small, but this dependence can possibly complicate the comparison of activation energies of diffusion for different experimental conditions, especially when considering that the activation energy itself might also depend on the temperature.

An additional point complicating the comparison of the measured temperature dependence is the different definitions used for the diffusion con-

stant. The above equation is used for both transport as well as self-diffusion, but the temperature dependence of these two quantities do not necessarily have to be the same. In addition, two different definitions are commonly used in literature for the transport diffusivity. The diffusion constant D_t, as encountered before, is defined directly by Fick's first law by considering the gradient of the total adsorbed phase in the crystals. Alternatively, Haynes and Sarma [24] proposed the use of a micropore diffusion constant D_x, assuming that most of the molecules are adsorbed on the pore wall and immobile, and only a small fraction is able to move with a diffusivity equal to this constant. These two diffusion constants can be related to each other via [25]

$$D_x = \varepsilon_x(1 + K_a)D_t \,, \tag{12}$$

in which ε_x is the porosity of the zeolite crystals and K_a is the equilibrium adsorption constant. In most cases $K_a \gg 1$, and D_x thus has an activation energy equal to the sum of the heat of adsorption and the activation energy for diffusion. Some questions, however, remain regarding the use of this diffusion constant, as in the narrow pores of the zeolite there is always a strong interaction between adsorbate and adsorbent, and a gas-phase cannot really exist in this environment. As a result, the distinction between a gas and adsorbed phase seems rather arbitrary, and the use of D_t as de diffusivity of the molecules is more appropriate.

1.3
Positron Emission and Positron-Electron Annihilation

The decay of radioactive isotopes via electron emission, so-called beta decay, is a well-known phenomenon. In this mode unstable nuclei that have an excessive number of neutrons, for example ^{14}C, can emit fast electrons, β^- particles, in order to attain a stable nuclear configuration. Nuclei with insufficient neutrons, such as ^{11}C, can obtain stability by emitting fast positrons, β^+ particles (the anti-matter equivalents of electrons). Both processes are classified as radioactive β decay. In each case, the mass number of the nucleus remains constant but the atomic number changes. There exist several positron emitting isotopes, of which ^{11}C, ^{13}N and ^{15}O in particular are of interest for catalytic reaction studies. Since the half-life time of these isotopes is only 20, 10 and 2 minutes, respectively, they must be produced on-site. Production of such radioactive isotopes is normally done by irradiation of an appropriate target material with protons or deuterons at high energy.

Since the positron is the antiparticle of the electron an encounter between them can lead to the subsequent annihilation of both particles. Their combined rest mass energy then appears as electromagnetic radiation. Annihilation can occur via several mechanisms: direct transformation into one, two, or three photons; or the formation of an intermediate, hydrogen-like bound state between the positron and the electron, called a positronium

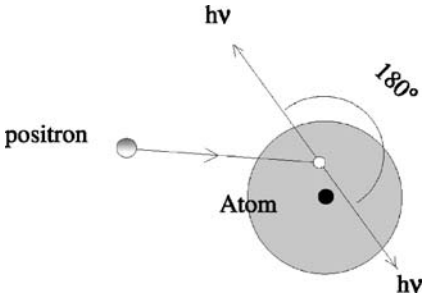

Fig. 4 Schematic drawing of the annihilation event

(Ps). The extent to that each annihilation mechanism contributes depends on the kinetic energy of the positron-electron pair. Positrons emitted during the β^+ decay process, possess a statistical distribution of kinetic energies ranging from zero to a maximum value, T_{max}, dependent on the decaying nucleus (T_{max} = 0.96 MeV for ^{11}C). The average kinetic energy is equal to 0.4 T_{max}. The probability of annihilation is negligibly small at high energies. The emitted positrons must therefore be slowed down by inelastic scattering interactions with the nuclei and the bound electrons within the surrounding medium to near thermal values before annihilation can occur. The lifetime of a positron is of the order of nanoseconds. During its lifetime the positron will travel a distance, known as the stopping distance, which is dependent on the energy of the positron and on the density of the surrounding material. For 0.4 MeV positrons (average kinetic energy of positrons emitted from ^{11}C) in a medium with a density of 0.5 g ml^{-1} (such as a zeolite or metal oxide) this corresponds to circa 3 mm [26]. The predominant annihilation process for thermalized positrons is via the direct production of two photons (Fig. 4). If both the positron and the electron were at rest upon annihilation, conservation of energy dictates that the energy of each emitted photon would be equal to the 511 keV, rest mass energy of the positron or electron. Conservation of momentum implies that the two gamma photons be emitted in opposite directions, since the initial momentum of the positron-electron pair was zero.

1.4 Positron Emission Detection Methods

The emitted gamma photons produced by positron-electron annihilation can be detected using scintillation crystal detectors such as sodium iodide (NaI), bismuth germanium oxide (BGO) and cerium doped lutetium oxyorthosilicate (LSO). The short half-life of most positron emitters leads to high specific activity. Only a very small quantity of radio-labeled molecules is thus required, making positron annihilation detection techniques very non-invasive. In fact, practical catalyst studies can be carried out using less than 37 kBq

of carbon-11, corresponding to less than 6.5×10^7 molecules. The first use of positron-emitting isotopes as tracers in catalysis research was published in 1984 by Ferrieri and Wolf [27, 28] for studying alkyne cyclotrimerization of acetylene and propylene. Baiker and co-workers [29] used ^{13}N-labeled NO to investigate the selective catalytic reduction (SCR) of NO by NH_3 over vanadia/titania at very low reactant concentrations.

For imaging purposes a technique based on the coincident detection of both photons produced via the annihilation event is often applied. This can be achieved by using two scintillation detectors, each placed on opposite sides of the emitting source. In this mode, only pairs of detected events that occur within a preset coincidence window (typically less than 50 ns) are counted. The position of the annihilation event that gave rise to the two detected photons can then be located along a chord joining the two detector elements. The concentration of the radio-labeled isotope at that position can also be determined by integrating the number of events detected during a fixed time. Due to the penetrating power of the emitted 511 keV gamma photons, which can pass through several millimetres of stainless steel, detection is possible from within steel reactors or process vessels. The coincident detection of photons is the principle of techniques such as, the positron emission tomography (PET), positron emission particle tracking (PEPT) and positron emission profiling (PEP).

Positron emission tomography (PET) is now well established as a diagnostic technique in nuclear medicine, providing 3D images of the distribution of radio-labeled molecules within living human organs. The development of a new breed of small self-shielding cyclotrons in the 1980s and significant improvements in computer hardware and software has led to an explosive growth in the number of PET facilities world-wide. Application of PET to problems of industrial interest has occurred only recently [30]. PET has been shown to be capable of monitoring turbulent two-phase (liquid/gas) flows using injected solutions of aqueous $Na^{18}F$ as a radiotracer [31].

Jonkers and co-workers conducted the first study in which PET was applied to chemical reactions in reactors [32, 33]. Since the early 1990s a facility has been developed at the Eindhoven University of Technology (TU/e) dedicated to positron emission imaging of physical and chemical processes in catalytic reactors at practical operating conditions. A positron emission detector has been developed that is specifically tailored to the measurement of activity distributions as a function of time along a single, axial direction, as a measurement of concentration profiles in a single dimension is sufficient under axially-dispersed plug flow conditions (since concentration gradients in the radial direction are negligible). This detector [34] is called a positron emission profiling (PEP) detector to distinguish it from its 3D parent.

The positron emission profiling (PEP) detector is shown in Fig. 5. It has been designed to be flexible, so that it can be used with a variety of different sizes of reactors. Measurements can be carried out on reactors having lengths

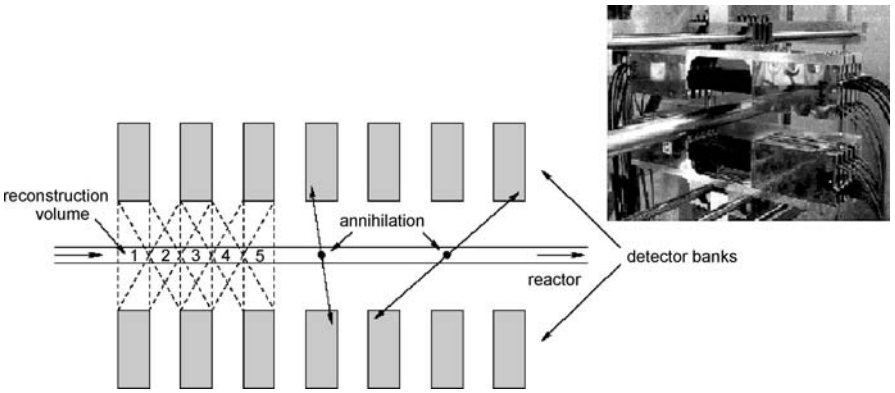

Fig. 5 Schematic drawing of the PEP detector with the two detector banks (not all detector elements are displayed). The first 5 (of 81) reconstruction positions are displayed. The photograph shows the PEP detectors with the stainless steel reactor between the two arrays of detectors

between 4.0 cm and 50 cm and diameters of up to 25 cm. The detector consists of two banks, each containing an array of 16 independent detection elements, and is mounted horizontally, with the reactor and furnace placed between the upper and lower banks. Each detection element is comprised of a bismuth germanium oxide (BGO) scintillation crystal coupled to a photomultiplier. The detection elements are situated in a frame, which allows adjustment of the overall detector dimensions if required.

2 Experimental

2.1 Diffusivity Measurements with PEP

The current PEP setup allows two types of experiments to measure diffusion in microporous materials. In the first type, labeled molecules are injected as a small pulse into a steady-state feed stream of either an inert carrier gas or of unlabeled molecules of the same kind. The propagation of the pulse through the reactor is followed using the PEP detector. Information about the diffusive processes can be obtained from the delay and broadening of the pulse, and quantitative information can be obtained by analysis of the measurements using an appropriate model, as will be discussed in more detail in the next section. This type of experiments is especially suited for diffusion measurements under zero loading conditions. A drawback of this method is that it is limited to the determination of single-component diffusion coeffi-

cients. Since under practical conditions multi-component diffusion occurs, a second method has been developed. In this type of experiments, called tracer-exchange PEP (TEX-PEP) [35], the labeled molecules are constantly "leaked" into the feed stream, instead of being injected as a single pulse. The PEP detector is used to measure the tracer exchange once the injection has started. By switching off the injection of labeled molecules after equilibrium is reached, the subsequent re-exchange can be followed as well. Information on the various processes can be obtained by fitting appropriate models to the time evolution of the tracer exchange at the various positions along the reactor bed. This technique will be applied to the study of binary mixtures. There are several advantages of the PEP technique over more conventional techniques. First of all, it is capable of measuring the concentration inside a packed bed reactor in situ [36]. Furthermore, PEP enables one to observe the evolution of a pulse or step change inside the reactor itself, therefore excluding the influence of reactor exit effects and minimizing the influence of entrance effects. Due to the penetrating power of the γ-photons used in the detection, no special requirements are being put on the experimental system holding the zeolite sample, and standard plugflow reactors can be used under typical conditions also found in the laboratory. Finally, the use of radiochemically labeled molecules makes this method particularly suited to study the diffusion of mixtures, as one of the components can be selectively labeled.

2.2 Experimental Setup

The positron-emitting ^{11}C isotope is produced by irradiation of a nitrogen target with 12 MeV protons from the 30 MeV AVF cyclotron at the Eindhoven University of Technology. The resulting ^{11}C is then transferred as CO/CO_2 to a special setup for the production of labeled hydrocarbons. Details of the homologation process over a Ru/SiO_2 catalyst used for the production of labeled pentanes and hexanes can be found in Cunningham et al. [37]. ^{11}C-labeled C_6 alkanes are synthesized from non-labeled 1-pentene, while non-labeled 1-butene is the starting material for ^{11}C-labeled C_5 alkanes production. After separation of the different products produced in this process, the desired labeled species is collected in a syringe.

Figure 6 shows a schematic diagram of the reactor system used for tracer-exchange positron-emission profiling (TEX-PEP) experiments. During these tracer exchange experiments, a constant flow of unlabeled hydrocarbons in a hydrogen carrier stream is fed into the reactor. The *n*-hexane/2-methylpentane/hydrogen mixture is generated in a dual CEM (controlled evaporator and mixer) system for feeding of *n*-hexane and 2-methylpentane. Each CEM unit consists of a liquid mass flow controller and a thermal gas mass flow controller, giving a controllable, constant flow of a liquid and a gas. The liquid is subsequently evaporated in a controlled manner in the mixing

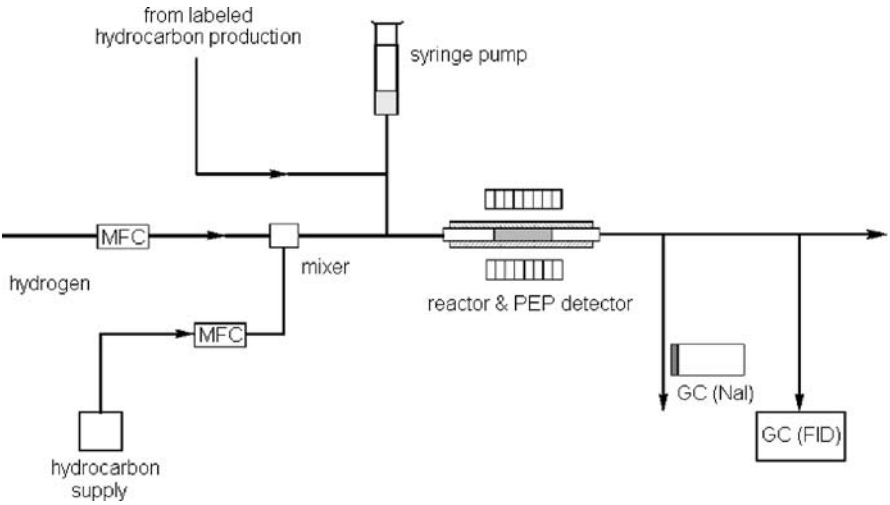

Fig. 6 Schematic layout of the TEX-PEP reactor setup including gas and liquid (unlabeled and labeled hydrocarbons) feed, the reactor and PEP detectors and post-reactor analysis. For diffusion measurements of binary mixtures a second liquid mass flow controller is added (MFC: mass flow controller)

unit of the CEM. We employ a total flow of hydrocarbons and carrier gas of 80.2 ml min^{-1}. In the TEX-PEP experiments, a quantity of labeled molecules of either *n*-hexane or 2-methylpentane is continuously injected into the feed stream using a syringe pump. The tracer exchange and tracer re-exchange processes are monitored by adding the very small tracer flow to the flow containing the non-labeled molecules until an equilibrium is reached and subsequently turning the tracer flow off. Due to switching effects [35], the re-exchange process yields more reliable results, and only this stage of the experiments was used for determining the kinetic parameters.

2.3 Zeolite Samples

All measurements in the present contribution have been performed on large crystals of silicalite-1 and H-ZSM-5 zeolites. Use of large zeolite crystals simplifies significantly the modeling and experimental procedure because it allows one to avoid pelletizing of the crystals. This has the important advantage that no macropore diffusion has to be included in the hydrocarbon transport models and intracrystalline diffusion is the dominating process.

The sample of silicalite-1 has been kindly supplied by Shell Research and Technology Center, Amsterdam. Scanning electron microscopy (SEM) showed that it consisted of regular coffin-shaped crystals with an average size of 150 $\mu m \times 50\ \mu m \times 30\ \mu m$. H-ZSM-5 has been kindly provided by

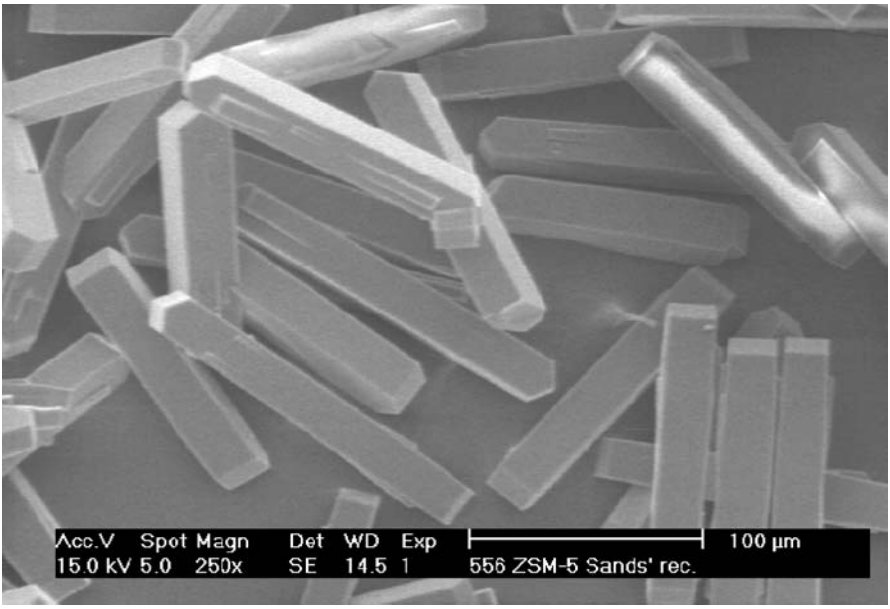

Fig. 7 SEM picture of H-ZSM-5 sample

Dr. L. Gora from Delft University. The average crystal size was determined with scanning electron microscopy and turned out to be 160 µm × 25 µm × 25 µm (Fig. 7). The Si/Al ratio was 40 in the initial gel composition. The concentration of the Brønsted sites equals 7.5×10^{-6} mol g^{-1} as determined by temperature-programmed isopropylamine decomposition. The bed porosity was determined from the pressure drop over the bed. From the Ergun relation a value of $\varepsilon = 0.44$ is calculated. The length of the zeolite bed was equal to 3 cm. Prior to experiments, the zeolite sample was activated for at least one hour at 673 K in a hydrogen stream.

2.4 Modeling the Tracer Exchange Process

In order to derive self-diffusion coefficients from the TEX-PEP experiments, a mathematical model is needed to describe the re-exchange process in the zeolite reactor bed. A common way to describe diffusion in packed beds is to use a set of diffusion equations, describing the mass transport in the zeolite bed and inside the crystals [3, 38, 39]. The model to analyze the TEX-PEP experiment study is basically a modification of the equations by Noordhoek et al. [25]. The process is thought to consist of the transport of molecules via convection and axial diffusion in the space between the crystals, adsorption and desorption at the zeolite crystal surface and diffusion inside the pores

of the crystals. It is assumed that the crystals have a spherical shape. This approximation is commonly made in literature and has been shown to be quite reasonable [3]. This is most probably due to the random orientation of the crystals inside the reactor, making it indeed difficult to explicitly account for the particle shape. As only one component is detected during the experiments, single-component equations can be used to model its behavior. The parameters describing the different processes in the bed will then be effective values for the transport of this component in the mixture.

2.4.1 The Model Equations

Transport in the fluid phase inside the packed bed takes place through convection, axial diffusion and flow to or from the zeolite crystals. A mass balance for a small volume element of the bed results in the following equation for the concentration c_z in the gas phase

$$\frac{\partial c_z}{\partial t} = D_{ax}\frac{\partial^2 c_z}{\partial z^2} - v_{int}\frac{\partial c_z}{\partial z} + \frac{3(1-\varepsilon)}{\varepsilon R_c}N_c \,. \tag{13}$$

In this equation, z is the coordinate along the reactor axis, D_{ax} is the axial diffusion coefficient and v_{int} the interstitial velocity, which can be calculated from the gas flow speed v_{sup} using $v_{int} = v_{sup}/\varepsilon$. The axial diffusivity can be calculated from the molecular diffusion coefficient of the component. For R_c, the radius of the crystals, the equivalent spherical particle radius is taken, defined as the radius of the sphere having the same external surface area to volume ratio [3]. We have estimated a value of 25 μm for the zeolite crystals in the current study.

The boundary conditions used for the bed equation are identical with the ones in Noordhoek et al. [25]. For the column entrance, a mass balance yields (and by neglecting the diffusional term just in front of the column)

$$\frac{\partial c_{z,0^+}}{\partial z} = \frac{v_{int}}{D_{ax}}(c_{z,0^+} - c_{z,0^-}) \tag{14}$$

in which $c_{z,0^-}$ and $c_{z,0^+}$ are the fluid phase concentrations just in front of and just after the column entrance, respectively. For TEX-PEP experiments, the concentration just in front of the packed bed is given by the Heaviside step function

$$c_{z,0^-}(t) = c_0, \quad t > 0 \tag{15a}$$

$$c_{z,0^-}(t) = 0, \quad t \leq 0 \tag{15b}$$

At the column exit, the diffusional term is neglected, turning into a first-order equation which can be used as a boundary condition.

The term N_c equals the mass flux through the boundary of the zeolite and is determined by the rate-limiting step for adsorption/desorption at the crys-

tal boundary. It is assumed that external mass transfer resistance due to the diffusion through the laminar fluid film surrounding the particles can be neglected, because this process is much faster than diffusion inside the zeolite crystals. This has been confirmed by comparing simulations with and without this process included in the model, showing that neglecting the external film mass transfer resistance does not influence the results.

The model of Nijhuis et al. [39] explicitly accounts for adsorption/desorption at the crystal boundary, assuming Langmuir adsorption kinetics. As the TEX-PEP experiments are conducted under steady-state conditions, this mechanism can be replaced by a simple first-order adsorption/desorption process

$$N_c = k_d c_x(R_c, z, t) - k_a c_z(z, t) \tag{16}$$

in which k_a and k_d are the adsorption and desorption rate constants in $[m\,s^{-1}]$. This equation furthermore has the advantage that k_a and k_d have the same dimensions and that there is no need to determine the number of adsorption sites.

Transport inside the zeolite crystals occurs through diffusion inside the zeolite pores. Although it is known that diffusion in zeolites is generally anisotropic [40], the random orientation of the crystals inside the reactor justifies the approximation that micropore diffusion can be described as an isotropic process. A mass balance for the zeolite crystals yields for the adsorbed phase concentration c_x in the crystals

$$\frac{\partial c_x}{\partial t} = D_c \left(\frac{\partial^2 c_x}{\partial x^2} + \frac{2}{x} \frac{\partial c_x}{\partial x} \right) , \tag{17}$$

in which D_c is the intracrystalline diffusivity, and x the radial coordinate of the crystal. In principle, the value of the diffusion constant depends on the concentration of both components. However, as during the experiments the total concentration does not change, D_c can thus be regarded as constant during a single measurement. The boundary condition at the center of the particle is obtained from symmetry considerations

$$\left. \frac{\partial c_x}{\partial x} \right|_{x=0} = 0 . \tag{18}$$

At the crystal boundary, the flow to the surface must be equal to the desorption rate at the crystal boundary at $x = R_c$

$$D_c \left. \frac{\partial c_x}{\partial x} \right|_{x=R_c} = k_a c_z(z, t) - k_d c_x(R_c, z, t) . \tag{19}$$

The initial conditions can be found by realizing that at the start of a tracer re-exchange process, the system is in equilibrium. Assuming that the injected tracer concentration initially is equal to C_0 yields the following initial

conditions

$$c_z(z, t) = c_0 \tag{20a}$$

$$c_x(x, z, t) = K_{ads} \cdot c_0 \,, \tag{20b}$$

in which K_{ads} is the adsorption equilibrium constant and equals $K_{ads} = k_a/k_d$.

2.4.2 Solving the Model

The equations described above have been solved using the numerical method of lines [41]. This procedure has been described for our system in more detail in Noordhoek et al. [36]. In short, this is done by discretizing the spatial coordinates and derivatives, converting the system of partial differential equations into a set of ordinary differential equations (ODEs). These ODEs can then be solved using an ordinary numerical integration routine. Solving the model yields values for the concentration at the each bed and crystal gridpoint. As the PEP detector measures the total concentration of labeled molecules in a certain section of the catalyst bed, volume averaging has to be applied to simulate the response of the PEP detector. The average microparticle concentration at position z inside the reactor bed equals

$$\langle c_x(z, t) \rangle = \frac{3}{R_c^3} \int_0^{R_C} c_x(x, z, t) \cdot x^2 \, dx \,. \tag{21}$$

As the crystal concentration c_x is only known at the gridpoints, this integral has to be evaluated numerically. The total concentration at position z can be calculated by averaging over the bed and crystal concentration

$$\langle c_{tot}(z, t) \rangle = \varepsilon c_z(z, t) + (1 - \varepsilon) \langle c_x(z, t) \rangle \,. \tag{22}$$

Estimation of the different parameters, i.e., the adsorption/desorption and diffusion in the zeolite crystals, is done by fitting the modeled concentration profiles to the measured ones, using the least-squares Levenberg–Marquardt algorithm [42]. All the other parameters were determined experimentally.

2.4.3 Adsorption/Desorption at the Crystal Boundary

If adsorption and desorption at the outer surface of the zeolite crystallites is fast compared to the diffusion inside the pores of the zeolite, adsorption equilibrium can be assumed at the crystal boundary. This seems a reasonable approach, because the diffusion inside the micropores is usually quite slow. An advantage of this approach is that the parameters describing adsorption/desorption at the boundary can be replaced by a single equilibrium ad-

sorption constant K_{ads}. This eliminates the problem that two parameters need to be fitted which are not completely independent, as was already reported by Nijhuis et al. [39]. In order to check whether the adsorption equilibrium assumption is satisfied, results for the model described previously are to be compared to those from a model assuming adsorption equilibrium. Based on the assumption that adsorption/desorption is fast compared to diffusion in the zeolite micropores, the mass flux through the boundary of the zeolite is determined by diffusion to the boundary of the crystal. Equation 15 is then replaced by

$$N_c = - D_c \left. \frac{\partial c_x}{\partial x} \right|_{x=R_c} . \tag{23}$$

The boundary equation at the crystal surface, Eq. 18, can be replaced by a simple equilibrium condition

$$c_x(R_c, z, t) = K_{ads} c_z(z, t) . \tag{24}$$

An estimate of the rate of adsorption can be obtained from kinetic gas theory [43]. The number of collisions between molecules and the surface can be calculated using the following relation

$$\Phi_s = \frac{1}{4} c_{gas} \sqrt{\frac{R_g T}{2\pi M}} , \tag{25}$$

which gives the collision rate per unit surface (in mol m^{-2}), with c_{gas} the concentration of the gas phase, R_g the ideal gas constant, T the temperature and M the molar mass of the molecules. The rate constant for adsorption can be calculated by dividing this expression by the gas phase concentration. It should, however, be realized that the value calculated from Eq. 24 gives an upper bound for the true adsorption rate, because not all collisions with the zeolite crystal surface will result in the adsorption of a molecule inside the micropores (i.e., there exists a "surface barrier" for adsorption, and the sticking coefficient is smaller than 1). Estimation of the sticking coefficient is not straightforward, and it might have values ranging from approximately one to 10^{-3}.

3
Diffusivity Studies of Hexanes in MFI Zeolites

3.1
Self-diffusivity of 2-Methylpentane/*n*-Hexane

The self-diffusivities of 2-methylpentane and *n*-hexane in their binary mixtures have been measured as a function of the ratio of the hydrocarbon in silicalite-1 at a temperature of 433 K. Figure 8 shows the tracer re-exchange

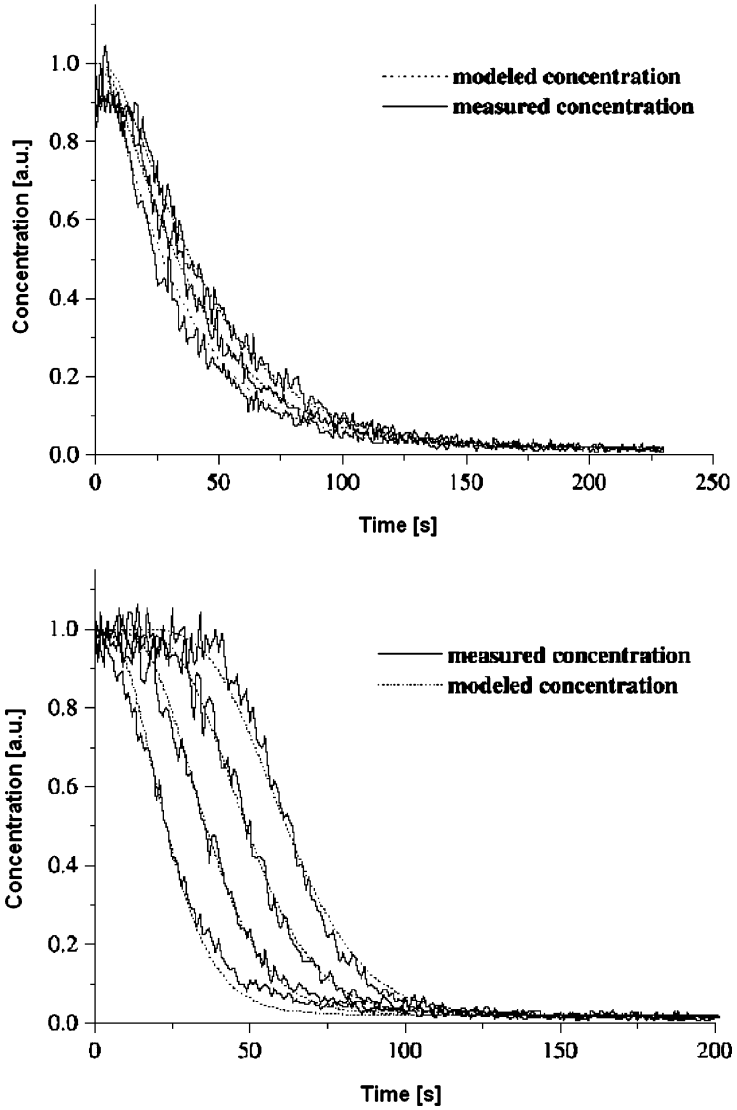

Fig. 8 TEX-PEP profiles for labeled 2-methylpentane (*left*) and *n*-hexane (*right*) at several detection positions in an equimolar mixture of *n*-hexane and 2-methylpentane in silicalite-1 at a total hydrocarbon pressure of 6.6 kPa and a temperature of 433 K (note that these two graphs have been obtained from two different experiments in which one of the two hydrocarbons was labeled)

process at different positions along the reactor axis for 2-methylpentane and *n*-hexane in an equimolar mixture. The results are derived from two different sets of experiments in which either the branched or the linear alkane was isotopically labeled. The data immediately show that the re-exchange process

of the branched molecule is slower than that of the linear hydrocarbon, indicating a correspondingly lower diffusivity for the former. Table 1 gives the hydrocarbon loadings of the two hydrocarbons on silicalite-1 at an adsorption temperature of 433 K.

The slightly lower loading of the branched alkane under equal experimental conditions is in accordance with other studies [44, 45]. Indeed, Zhu et al. [45] measured a higher *n*-hexane loading in silicalite-1 compared to 2-methylpentane even under a significantly higher partial pressure of the iso-alkane. The *n*-hexane loading at a partial pressure of 0.47 kPa and a temperature of 408 K was found to be 2.36 molecules per unit cell, while a value of 2.28 was calculated for 2-methylpentane at a partial pressure of 0.73 kPa. Loadings for both *n*-hexane and 2-methylpentane determined from the independent experiments using a mass spectrometer (MS) are in agreement with those provided by TEX-PEP (see Table 1).

Table 1 Loadings of single components in silicalite at 433 K, 6.6 kPa

Hydrocarbon	Loading [mmol g^{-1}]	Loading [molec. uc^{-1}]	Loading [mmol g^{-1}] (MS)
n-hexane	0.64 ± 0.03	3.6	0.59 ± 0.03
2-methylpentane	0.59 ± 0.03	3.4	0.53 ± 0.03

Theoretically calculated values of the heat of adsorption for *n*-hexane and 2-methylpentane are 70 kJ mol^{-1} and 65 kJ mol^{-1}, respectively [46, 47], which is in agreement with the average values determined by Zhu et al. [48]. As the heats of adsorption of these alkanes are very close, the difference in adsorption is caused by an entropic effect. Indeed, the conformations of the bulkier branched alkanes are much more restricted in the narrow pores of the medium-pore MFI zeolite. For the branched isomer in silicalite-1 there is a large difference in the adsorption entropy between the molecular locations in the intersections and in the channels as shown by Zhu et al. [48]. Therefore, the adsorption of 2-methylpentane from the gas phase leads to a higher reduction in entropy compared to adsorption of *n*-hexane. This makes it entropically less favorable to adsorb the branched isomer [44].

Figure 9 shows the binary adsorption data of *n*-hexane and 2-methylpentane at 433 K as a function of the gas-phase ratio of the hydrocarbons. Obviously, the *n*-hexane loading monotonically decreases upon an increase of the partial pressure and loading of the 2-methylpentane. The total hydrocarbon loading only slightly decreases at high 2-methylpentane fraction in the gas phase. The preference for adsorption of *n*-hexane over the monobranched isomer is in line with the above-mentioned entropic considerations.

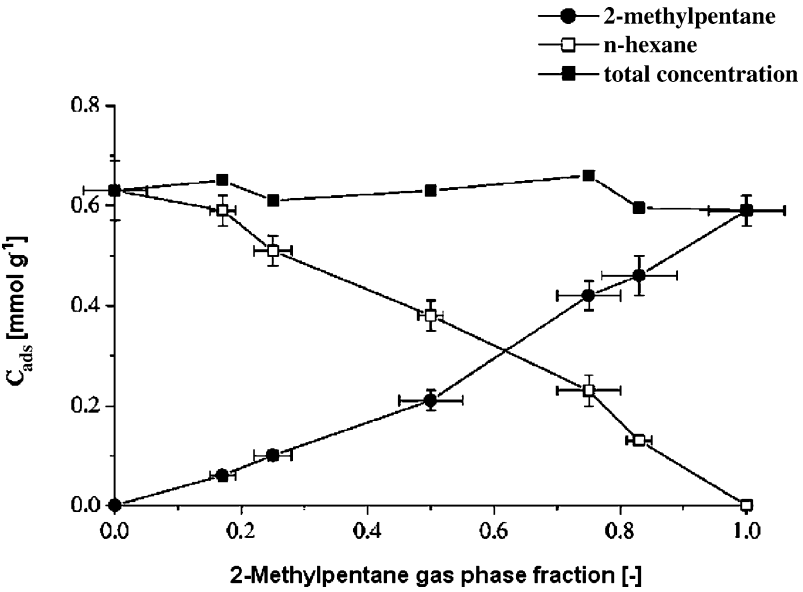

Fig. 9 Loadings of mixture components in silicalite as a function of 2-methylpentane fraction in the gas phase (total hydrocarbon partial pressure 6.6 kPa, $T = 433$ K)

The observations in the present study are supported by results of CBMC simulations performed by Vlugt et al. [44] and Calero et al. [49] on adsorption behavior of linear and branched alkanes and their mixtures. The simulations were performed at a fixed mixture ratio at lower temperatures (300 K and 362 K). It was shown, that at a total loading of approximately 4 molecules per unit cell, the loading of the branched alkanes reaches a maximum value. At lower loadings, both components are adsorbed independently, while at higher loadings the branched alkanes is squeezed out by the linear alkanes. Vlugt et al. [44] showed that this behavior of the component is related to the siting of the molecules in the silicalite pore system. It was found that the *n*-hexane is adsorbed throughout the silicalite-1 pores, whereas 2-methylpentane molecules are located mostly at the intersections between the straight and zigzag channels. Consequently, *n*-hexane displays a higher packing efficiency. Apparently, under the present conditions, the loading of the components were quite high, so that the 2-methylpentane is expelled from the micropores and a preferential adsorption for the linear alkane is observed. This effect can only be counteracted at high partial pressures of 2-methylpentane. This results in substantial nonlinear dependencies of the loadings on the mixture composition. Comparison between our experimental results and those calculated from CBMC simulations [50] performed for 2-methylpentane/*n*-hexane mixtures under almost similar conditions is shown in Fig. 10. The single-component loadings of the single components

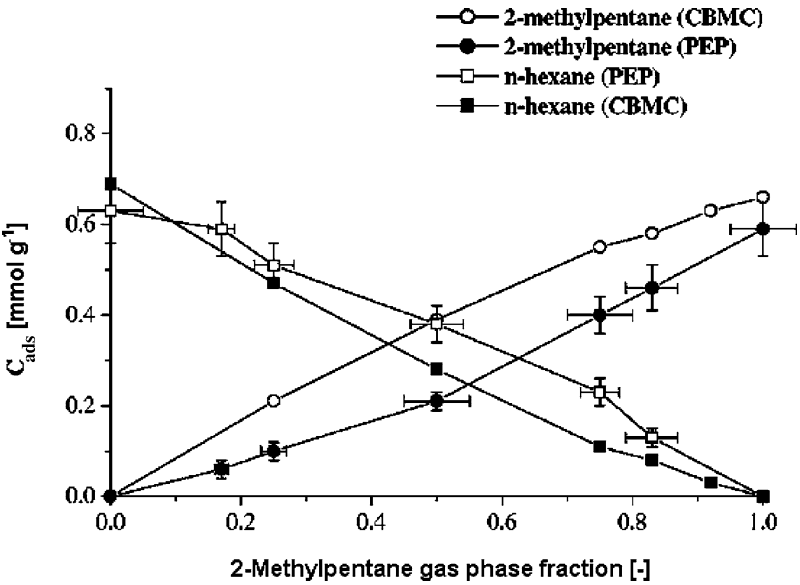

Fig. 10 Loadings of mixture components in silicalite as a function of 2-methylpentane fraction in the gas phase, experiment (total hydrocarbon partial pressure 6.6 kPa, 433 K) and CBMC simulations (total hydrocarbon partial pressure 7.8 kPa, 433 K)

calculated by CBMC simulations are slightly higher than the values obtained from TEX-PEP measurements.

This is more evident for the branched alkane and is related to the higher hydrocarbon partial pressures applied in the CBMC simulations. The slight decrease of the total loading with the branched alkane fraction in the gas phase predicted from the simulations is in agreement with the TEX-PEP data. However, a slight preferential adsorption for the branched alkane is deduced from the simulations, whereas PEP measurements provide lower values for the 2-methylpentane loadings. This disagreement and the tendency shown by Vlugt et al. [44] can probably be attributed to imperfections in the model parameters used in the CBMC simulations.

Figure 11 shows the self-diffusion coefficients obtained from the TEX-PEP experiments for both alkanes as a function of the gas-phase mixture composition. Evidently, we find that the self-diffusivity of *n*-hexane is an order of magnitude higher than that of the 2-methylpentane. Indeed, the kinetic diameter of *n*-hexane (4.3 Å) is smaller than that of isohexane (5.0 Å) [51]. Moreover, we observe a decrease in mobility with increasing fraction of the branched alkane in the gas phase. Analogous behavior was found for CH_4/CF_4 mixtures, where the self-diffusivity of both components decreased as the loading of the slower diffusing tetrafluoromethane increased [52].

The loading dependence of 2-methylpentane is similar to earlier results showing a decrease of 2-methylpentane diffusivity with loading in single-

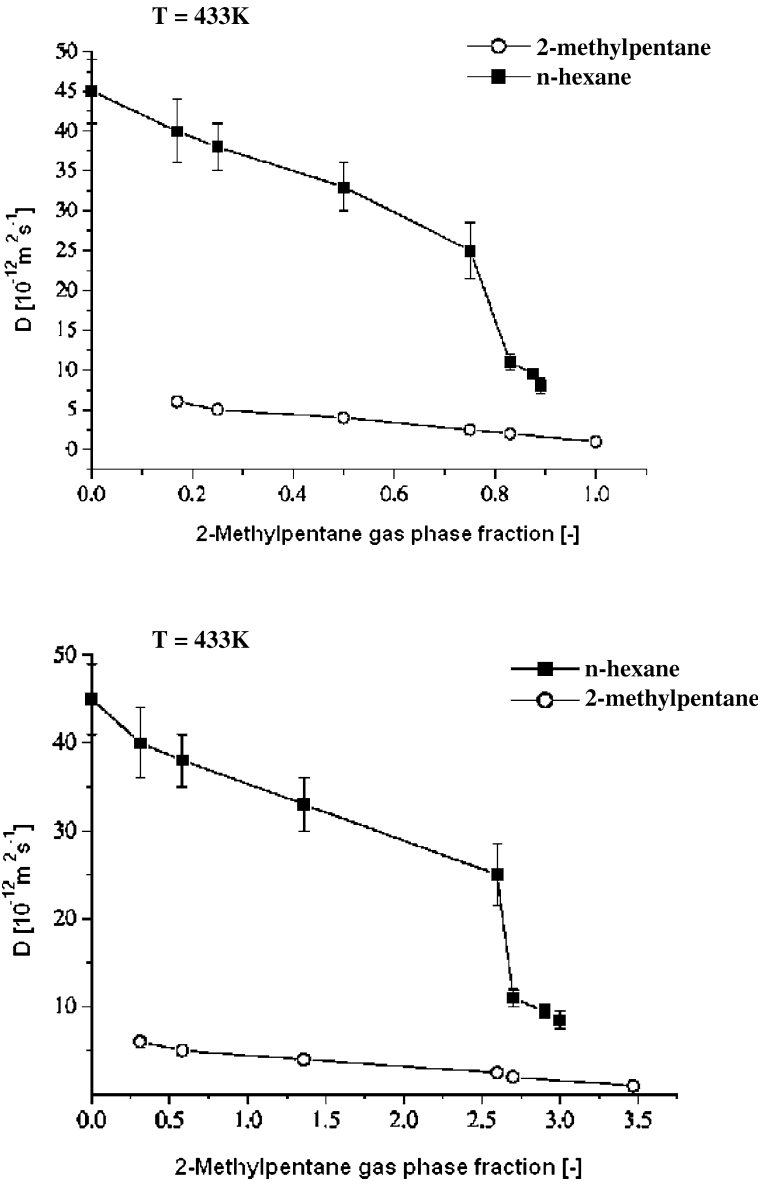

Fig. 11 Self-diffusivities of mixture components in silicalite as a function of the 2-methylpentane fraction in the gas phase (*left*) and as a function of the 2-methylpentane loading (total hydrocarbon pressure 6.6 kPa, 433 K)

component studies [53] and indicating that the mobility of the slower component is not noticeably affected by the presence of a fast one [54–56]. A peculiar observation is found in the dependence of the *n*-hexane self-diffusivity on

the 2-methylpentane fraction. We find a monotonous decrease of the self-diffusivity with an increase of the isohexane fraction up to a value of 0.75. At higher values a strong decrease in the linear alkane diffusivity is observed, and the values for the self-diffusivity of *n*-hexane and 2-methylpentane become close. This sharp drop in mobility results from the hindrance imposed by its branched isomer, because the total loading remains more or less constant. Diffusion in zeolites is considered to proceed via a sequence of activated jumps from one site to the other. A jump is successful if the neighboring site to which the molecule attempts to jump is empty. Isohexane molecules are preferentially adsorbed at the channel intersections that connect the straight and zigzag channels. An increase of the amount of slowly moving molecules (2-methylpentane) will lead to the blockage of these intersections. Thus, the number of successful jumps of the fast component (*n*-hexane) should be determined by the rate at which an empty site is created by a jump of the slow component. Thus, at high loadings of 2-methylpentane, the self-diffusivity of *n*-hexane becomes strongly determined by the self-diffusion rate of its branched isomer. In Fig. 11, the self-diffusion coefficients of both components are shown as a function of the 2-methylpentane loading. One can see that the sudden drop in *n*-hexane diffusivity occurs at a 2-methylpentane loading of approximately 2.75 molecules per unit cell. We surmise that this loading already blocks the three-dimensional pore network of silicalite-1 strongly enough to lead to considerably lower *n*-hexane diffusivities. When all the intersections are occupied by the slowly diffusing branched alkanes, the entire pore system will be blocked. As a consequence of this, the diffusion of hexane will be determined by the diffusion rate of the slow component. Indeed, when the loading of 2-methylpentane increases further, *n*-hexane diffusivity continues to decrease, and one would expect them to become equal at higher loadings. Similar phenomena regarding the blockage of the pore network were observed during the adsorption of methane and benzene in zeolite Na-Y [57] and silicalite [58]. In Na-Y, the benzene molecules block the windows of the supercages and disrupt the mobility of the smaller methane molecules. Förste et al. [58] showed that the decrease of methane diffusivity was also caused by blocking of the channel intersections by benzene in MFI zeolite. For methane/xenon mixtures in silicalite-1, both components are preferentially sited in the interiors of the (straight and zigzag) channels, causing the blocking by the slow components to be less dramatic [54].

For *n*-butane/methane [56] and methane/tetrafluoromethane [52] mixtures in silicalite, a decrease in the diffusivity of both mixture components was observed with an increase of the loading of slower *n*-butane and methane. In the first case, methane shows a preferential adsorption for the intersections, while *n*-butane is approximately equally adsorbed in the straight and zigzag channels [46]. In mixtures of CH_4/CF_4 in silicalite, CF_4 adsorbs preferentially in the straight channels while methane adsorbs in zigzag channels. The decrease in diffusion rates for these components is probably caused

by the decrease of the probability for the molecule to jump to a free neighboring adsorption site. A sharp drop in the diffusivity was indeed observed by Masuda et al. [55], who studied binary diffusion of *n*-heptane and *n*-octane in silicalite. These alkanes do not have any preference for a particular adsorption site. Therefore, both components (the faster and the slower one) will diffuse on a rate similarly decreased upon increased loading. Thus, multicomponent diffusion is not only strongly related to the zeolite topology and adsorption properties of the components, but also by the presence of another adsorbate. The diffusion coefficient of a component will then also depend on the loading of the other component. This makes it crucial to obtain more insight into multicomponent diffusion coefficients because in most practical situations diffusivity will be determined by the mixture components and relative concentrations.

3.2 Influence of Acid Sites on Diffusivity: a Comparison of Silicalite-1 and H-ZSM-5

In the previous section we investigated the diffusivity of *n*-hexane and 2-methylpentane in an all-silica MFI zeolite. To obtain more insight into the role of acidity we compare here results obtained with silicalite-1 and H-ZSM-5. The loadings of both components in silicalite-1 and H-ZSM-5 are displayed in Fig. 12. The adsorbed concentration of *n*-hexane in H-ZSM-5 is higher than in silicalite-1. This result should be expected from the presence of the acid sites, since the enthalpy of *n*-hexane adsorption in H-ZSM-5 (82 kJ mol^{-1}) was reported to be higher than in silicalite-1 (72 kJ mol^{-1}) [59]. For isohexane these values were reported to be lower by 6 kJ mol^{-1}. It was found that in H-ZSM-5 at high *n*-hexane loadings a complex of two hydrocarbon molecules with the bridging hydroxyl group is formed, whereas isoalkane molecules are unable to form such a complex with the acid site. Indeed, in our study 2-methylpentane loadings in mixtures in H-ZSM-5 are very close to those in silicalite-1.

The loading of *n*-hexane in mixtures is somewhat higher than it is expected to be if it were proportional to its partial pressure (Fig. 12). On the contrary, the 2-methylpentane loading is somewhat lower. This points to preferential adsorption of *n*-hexane over isohexane in their mixtures in H-ZSM-5 than in silicalite-1. In earlier experimental [50] and CBMC simulation studies [44] of *n*-hexane/isohexane mixtures in silicalite-1, a slight preferential adsorption of the linear alkane over the branched one has been found. The most prominent explanation for this preference is the molecular siting of these two hydrocarbon molecules. Whereas *n*-hexane exhibits no clear preference for a position in the micropore system of MFI zeolite, the branched isomer is preferentially located at the channel intersections due to entropic reasons [44]. Consequently, 2-methylpentane will be pushed out from silicalite-1 by *n*-hexane. These effects are even stronger for H-ZSM-5, most likely due to the stronger

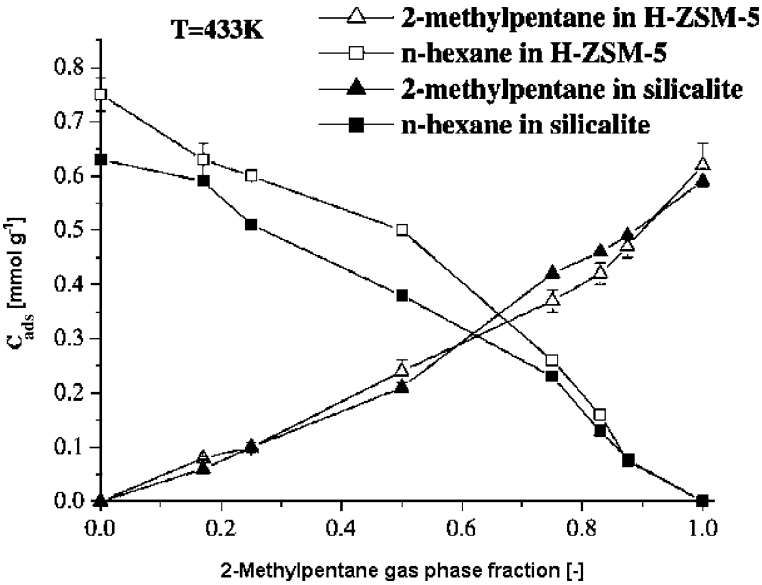

Fig. 12 Loadings of mixture components in both MFI-type zeolites as a function of 2-methylpentane fraction in the gas phase, total hydrocarbon pressure 6.6 kPa, 433 K

interaction of *n*-hexane with acid sites than the branched alkane [59], which results in a higher packing efficiency for the linear alkane (Table 2).

Table 2 shows the adsorbed concentrations of the pure components. At a partial pressure of 6.6 kPa the amount of *n*-hexane is just slightly higher than that of isohexane in silicalite-1, while the linear alkane is obviously adsorbed more strongly than 2-methylpentane in H-ZSM-5 due to the stronger interaction with the acid sites. The maximum loading of each component has been measured by a separate adsorption study. The sorption capacity of *n*-hexane (7 molecules per unit cell), in agreement with earlier studies [48, 59–61] exceeds that of 2-methylpentane (4 molecules per unit cell). The latter value equals the number of channel intersections in the MFI pore system per unit cell. Indeed, the sorption of isohexane molecules at

Table 2 Loadings of single components (mmol g^{-1}) in silicalite-1 and H-ZSM-5 at 433 K (loadings given at a hydrocarbon partial pressure of 6.6 kPa and the maximum loading)

Zeolite	*n*-hexane 6.6 kPa	c_{max}	2-methylpentane 6.6 kPa	c_{max}
H-ZSM-5	0.75	1.1 ± 0.2	0.62	0.74 ± 0.04
silicalite-1	0.63	1.2 ± 0.2	0.59	0.75 ± 0.02

energetically less favorable locations requires high pressures [44]. An experimental study of single-component *n*-butane and isobutane adsorption by the volumetric method in silicalite-1 and H-ZSM-5 leads to similar conclusions [62]. Valyon et al. [62] found that under identical conditions the *n*-butane loading was 1.5 (2.0) times higher than that of isobutane at a temperature of 273 (413) K. For H-ZSM-5 complete saturation with butanes was reached at lower pressures because of the stronger interactions with the acid sites. For *n*-butane the maximum loading was found to be equal to approximately 8 molecules per unit cell, while for isobutane the inflection in the isotherm was observed at a sorbed amount of 4 molecules per unit cell. Our results support the finding that the stronger interaction of linear alkanes with acid protons in H-ZSM-5 compared to branched ones results in a preferential adsorption of linear *n*-hexane over 2-methylpentane.

Figure 13 displays the self-diffusivities of *n*-hexane and 2-methylpentane in silicalite-1 and H-ZSM-5 as a function of the ratio of the hydrocarbons. The self-diffusivities of both hexanes linearly decrease with increasing gas-phase fraction of the branched hexane in the gas phase for the non-acidic and acidic zeolite. In H-ZSM-5, the mobility of alkanes is approximately two times slower than in silicalite-1. Obviously, the presence of acid sites strongly affects the molecular transport due to stronger interactions with the *n*-hexane molecules. A similar effect of Brønsted sites on the single component diffusion of aromatics was observed in MFI zeolites with different concentration of acid sites [63–65]. The *frequency response* (FR) technique provided similar results

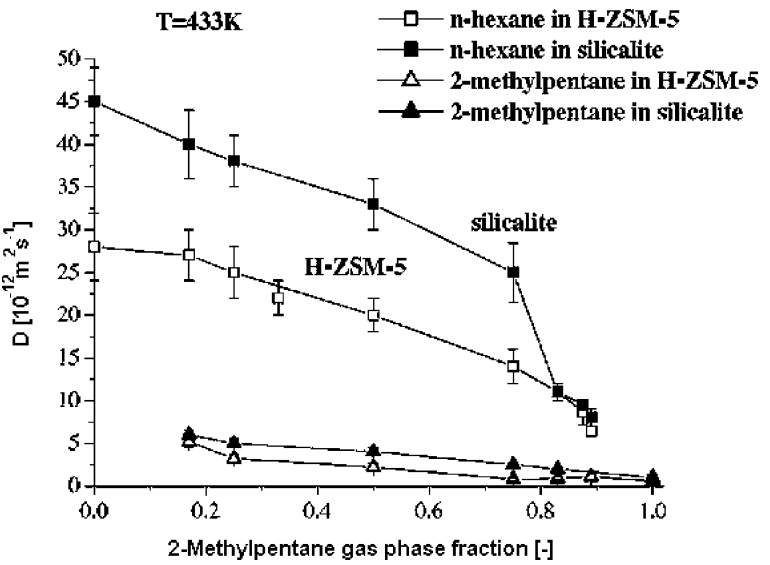

Fig. 13 Self-diffusivities of mixture components in both MFI-type zeolites as a function of 2-methylpentane fraction in the gas phase (total hydrocarbon pressure 6.6 kPa, 433 K)

for *n*-butane and isobutane diffusion in silicalite-1 and H-ZSM-5 [62]: the diffusivity of both components was approximately half in the acidic zeolite sites and the diffusion of isobutane was significantly slower compared to *n*-butane.

In the present study of binary mixtures the self-diffusivity of the faster component (*n*-hexane) in H-ZSM-5 is influenced by two factors: (i) the presence of slower 2-methylpentane molecules and (ii) the strong interaction of the linear alkane with acid sites. As long as the concentration of the branched hexane does not exceed a critical value, the effect of the Brønsted sites is dominating and the diffusion of *n*-hexane in mixtures is roughly two times lower in H-ZSM-5 than in the zeolite without acid sites. A behavior similar to that of *n*-hexane is observed for 2-methylpentane in Fig. 13. Its self-diffusivity decreases in both zeolite-types with increasing loading and analogous to *n*-hexane the self-diffusion coefficient in H-ZSM-5 is half that in silicalite-1, even for the single-component experiment. Thus, the presence of the Brønsted sites noticeably decreases the diffusivities of both hexanes due to the increased hydrocarbon-zeolite interaction in the presence of protonic sites.

Around a value of the gas-phase fraction of 2-methylpentane of about 0.83, the influence of the acid sites on the *n*-hexane diffusivity is not dominant anymore in comparison to the pore occupation of slow-diffusing 2-methylpentane. Figure 14 shows the dependence of the diffusivities of both components versus the concentration of adsorbed 2-methylpentane in terms of molecules per unit cell. The diffusivities of *n*-hexane in silicalite-1 and H-ZSM-5 become nearly equal when the concentration of 2-methylpentane reaches approximately 2.75 molecules per unit cell. For 2-methylpentane we find that the self-diffusivity in silicalite-1 becomes very close to the value in H-ZSM-5 at the same loading.

Earlier we discussed the behavior of binary mixtures of linear and monobranched hexanes in silicalite-1. We found that pore blockage due to preferential adsorption of the branched isomer occurs when its concentration reaches approximately 2.7 molecules per unit cell. From CBMC simulations [44] it is known that monobranched molecules such as 2-methylpentane and 3-methylpentane prefer to occupy the intersections between straight and zigzag channels in MFI-type zeolites. On the other hand, from its crystallographic zeolite structure [1] we know that the MFI unit cell has four intersections. Therefore, the diffusivity of *n*-hexane sharply decreases when more than half of the intersections are occupied by its branched isomer. Figure 14 shows that a further increase of the 2-methylpentane loading up to three molecules per unit cell results in the *n*-hexane diffusivities in silicalite-1 and H-ZSM-5 becoming almost similar. This can be explained by the influence of the co-adsorbed branched isomer. While the acid sites in H-ZSM-5 slow down *n*-hexane diffusivity considerably, this effect is largely absent when 2-methylpentane is present in the micropores. Our observations are confirmed by a recent experimental study of diffusion in silicalite of binary mixtures of alkanes (*n*-heptane, *n*-octane) and aromatics (ortho- and

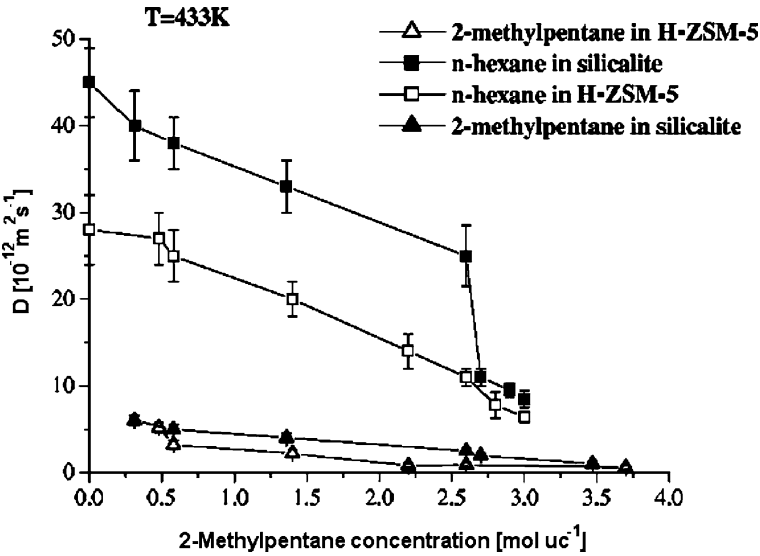

Fig. 14 Self-diffusivities of mixture components in both MFI-type zeolites as a function of 2-methylpentane loading, 433 K

meta-xylene) [55]. These authors found that a component with a low diffusion coefficient can considerably slow down diffusion of a faster one by selective blocking of the zeolite intersections [65]. They also measured that the diffusion of the slow component is not affected by the presence of the fast component, which is in agreement with studies of methane/xenon mixtures [66]. This is also in agreement with our study.

Summarizing, we conclude that for binary mixtures of a linear and branched hexane in H-ZSM-5 and silicalite-1 two factors influence the respective diffusivities: (i) the strong interaction with acid sites preferentially decreases *n*-hexane diffusivity and (ii) the blocking of intersection adsorption sites by 2-methylpentane decreases *n*-hexane diffusivity. At high loadings of the branched isomer the latter effect is dominating, and finally the diffusivity of the linear hexane is totally determined by its branched isomer.

The current work indicates the strong effect of acid sites on the interaction and diffusivity of hydrocarbons. To further study this effect, we determined the single-component diffusion coefficients and specifically the activation energy for diffusion. Activated diffusion is described by the Arrhenius-type Eq. 8. The pre-exponential factor D_{inf} is related to the jump frequency between adsorption sites in the zeolite lattice, while the exponential expresses the chance that the molecules are able to overcome the free energy barrier E_{act} between these sites. The loadings of *n*-hexane and 2-methylpentane in H-ZSM-5 and silicalite-1 have been measured at temperatures between 373 and 533 K at intervals of 20 K. The hydrocarbon pressure was taken identical

to that in the binary mixture experiments (6.6 kPa). The values of the apparent activation energies for diffusion have been obtained. The term *apparent* activation energy of diffusion (E_{app}) is explicitly used to distinguish it from the *true* activation energy of diffusion (E_{act}). The latter activation energy is determined at constant (mostly very low) concentration of the adsorbate. However, in the present experiments a change in temperature not only leads to a change in the diffusion coefficient but also in the adsorbate loading.

Figure 15 displays the loadings of *n*-hexane and 2-methylpentane in both zeolites. Under similar conditions, the adsorbed concentration of *n*-hexane is higher than that of 2-methylpentane, especially at lower temperatures. The interaction with *n*-hexane results in higher loadings for H-ZSM-5 than for silicalite-1. From the temperature dependence of the diffusivity of *n*-hexane in both zeolites, the apparent activation energy has been deduced and the results are collected in Table 3. Corresponding Arrhenius plots are shown

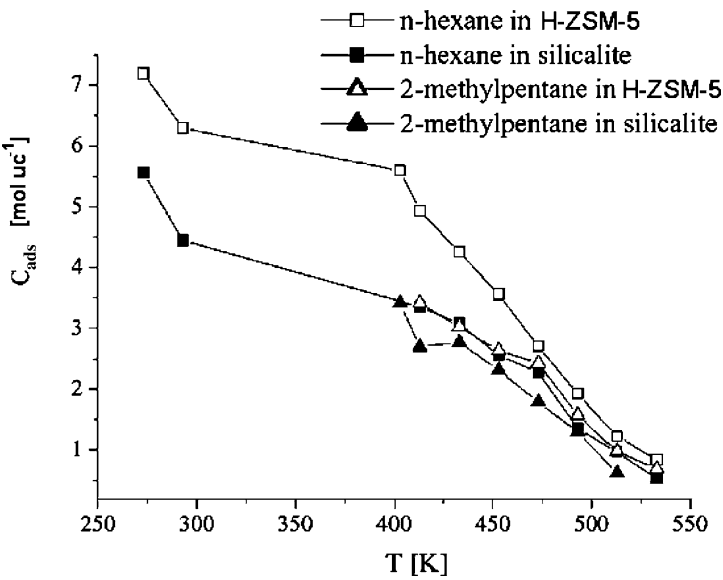

Fig. 15 Loadings of hexanes measured at various temperatures in silicalite-1 and H-ZSM-5

Table 3 Apparent activation energy of diffusion for *n*-hexane in MFI-type zeolites and a comparison with literature

Zeolite	E_{app} [kJ mol^{-1}] TEX-PEP	Refs.
Silicalite-1	18.5 ± 1.5	16–19 [73–75]
H-ZSM-5	22.0 ± 2.0	20–24 [67–69]

in Fig. 16. The apparent activation energy measured with the TEX-PEP is higher for H-ZSM-5 than for silicalite-1, although the difference is small and not totally significant. Experiments earlier performed at 433 K show that

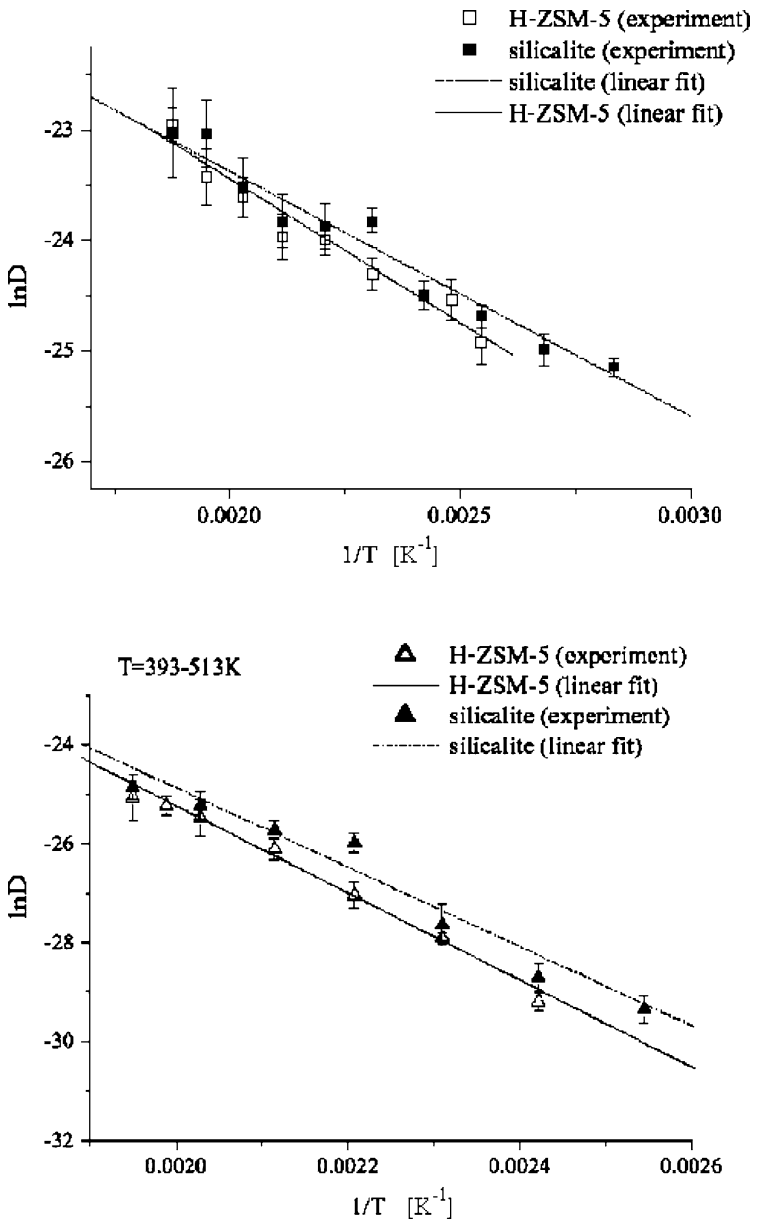

Fig. 16 Arrhenius plots for diffusivities of *n*-hexane (*left*) and of 2-methylpentane (*right*) in silicalite-1 and H-ZSM-5

the diffusivity of *n*-hexane in H-ZSM-5 is by a factor of two lower than in silicalite-1. Valyon et al. [62] have measured the activation energy of diffusion for *n*-butane in silicalite-1 and H-ZSM-5 with the FR method. They found values of 10.7 and 13.1 kJ mol^{-1} respectively, which explained the increase of hydrocarbon diffusivity in the absence of protonic sites. In our case we also find a higher activation energy for the acidic material. The values are in good agreement with values provided by other techniques (Table 3). The activation energy of *n*-hexane diffusion in H-ZSM-5 determined by the FR method [67, 68] is equal to 24 kJ mol^{-1}. The constant volume method provided a value of 20 kJ mol^{-1} [69]. Thus, a value of 22 ± 2 kJ mol^{-1} as measured in this work overlaps very well with these values. On the other hand, Hermann et al. [70–72] found a somewhat lower value of 15.6 kJ mol^{-1} upon measurements of the transport diffusivity of *n*-hexane in H-ZSM-5 at relatively low loading by a micro-FTIR technique.

The value of the apparent activation energy for silicalite-1 is also reproduced by other methods such as the ZLC and the square wave methods [73–75]. Discrepancies, however, occur with techniques such as membrane permeation and TEOM, that provided somewhat higher values of the activation energy for *n*-hexane, i.e., 34.7 kJ mol^{-1} [76] and 38 kJ mol^{-1} [45], respectively. In the membrane permeation technique very high loadings up to eight molecules per unit cell were used, which may explain the discrepancy. The value provided by Zhu et al. [45] is the activation energy deduced from the corrected diffusivities. The diffusivities were measured at different conditions (partial pressures) and the loadings were also up to 5.25 molecules per unit cell.

In principle, one would expect an increase in the activation energy of diffusion in the presence of the acid sites. The interaction of the hydrocarbon with Brønsted sites will increase the barrier to be overcome for hopping of the hydrocarbon from one to the next site. Indeed, this is observed by several authors, although we should note that the effect is generally small compared to the accuracy of the measurements.

Corresponding Arrhenius plots for the diffusion of 2-methylpentane in silicalite-1 and H-ZSM-5 are presented in Fig. 16, and the results are collected in Table 4. The diffusivities have been measured in the temperature interval

Table 4 Apparent activation energy of diffusion for 2-methylpentane in MFI-type zeolites and a comparison to literature data

Zeolite	E_{app} [kJ mol^{-1}] TEX-PEP	Refs.
Silicalite-1	66 ± 6	50 [45]; 46 [77]
H-ZSM-5	72 ± 3	24 [79]; 36 [78]

393–513 K and 413–533 K for silicalite-1 and H-ZSM-5, respectively. An experimental problem is the low concentration of adsorbed 2-methylpentane at higher temperatures which leads to a low signal-to-noise ratio. This prohibits us to measure the diffusivity and the loading of 2-methylpentane in silicalite at 533 K. For the same reason the experimental error was slightly higher than 10% for the other measurements. The apparent activation energies of diffusion found for 2-methylpentane in silicalite-1 and H-ZSM-5 are both significantly higher than those for *n*-hexane. This results in an order of magnitude difference in the diffusion coefficients for these alkanes. This is in agreement with the earlier studies of linear and mono and dibranched alkanes in MFI-type zeolites [77, 78].

The commonly accepted explanation for the higher activation energies of diffusion for isoalkanes in MFI zeolites is that due to its higher critical diameter isoalkanes experience a steric hindrance during diffusion. Similar to *n*-hexane, we find a higher value for the apparent activation energy of 2-methylpentane in H-ZSM-5 than in silicalite-1. This is in agreement with the findings of the FR technique for isobutane diffusion in MFI-type zeolites [62]. The activation energy of isobutane was measured to be 1.2 kJ mol^{-1} higher in H-ZSM-5. TEX-PEP does not allow us to be that precise in this case, but in combination with data on mixture experiments we suggest that the interaction between the alkane and the Brønsted sites results in an increase in the activation energy of diffusion. The values for the activation energy for 2-methylpentane diffusion in both zeolites measured here are significantly higher than those measured by other techniques (Table 4). TEOM [45] and gravimetric measurements [77] provide an activation energy for branched hexane diffusion in silicalite-1 of 50 and 46 kJ mol^{-1}, respectively. This value is even higher than that obtained in H-ZSM-5 as measured by Xiao and Wei with the same method (36 kJ mol^{-1} [78]) and by Keipert and Baerns with a transient technique (24 kJ mol^{-1} [79]).

The discrepancies between the values of the activation energies provided by different authors can be attributed to the different alkane partial pressures. Several theoretical and experimental studies indicate a significant concentration dependence of diffusion in zeolites [4, 19, 77, 78, 80]. Coppens et al. [19] have shown for MFI zeolite with Monte-Carlo simulations that the diffusivity can drop by a factor of ten when the occupancy is close to saturation. In this work we performed our experiments under a hydrocarbon partial pressure of 6.6 kPa, which is higher than the pressures in TEOM, gravimetric and volumetric measurements.

Figure 15 shows the loadings of 2-methylpentane and *n*-hexane in both zeolites in the temperature interval used to determine the activation energy. The loading of 2-methylpentane reaches 3.5 molecules per unit cell with the loadings in H-ZSM-5 being slightly higher than in silicalite-1 at the same temperatures. The maximum loadings of 2-methylpentane in silicalite-1 and H-ZSM-5 were measured to be 0.75 mmol g^{-1}, which corresponds to approxi-

mately 4.2 molecules per unit cell. At a partial pressure of 6.6 kPa, the zeolite loading was up to 80% of the saturation, which is higher than the experimental conditions of other techniques. Indeed, in the transient experiments performed with a TAP reactor [79] a pulse of a very small amount of molecules is admitted to the empty zeolite. In such a case the influence of other hydrocarbons can be excluded. It is also important to note that the experimental conditions (partial pressure) used in the gravimetric experiments [77, 79] were not specified. Nevertheless, diffusion coefficients provided by those techniques are in a fair agreement with the values measured here. The data are collected in Table 5.

Table 5 Diffusion coefficients for 2-methylpentane in MFI-type zeolites and a comparison with literature

Zeolite	D [$m^2 s^{-1}$] (T = 423 K)			
	Grav. [74, 75]	Grav. [76]	TAP [77]	PEP
Silicalite-1	2×10^{-12}			1.1×10^{-12}
H-ZSM-5		9×10^{-13}	1×10^{-12}	4×10^{-13}

Summarizing, we observe that the presence of acid sites causes a decrease in the self-diffusivity of *n*-hexane and 2-methylpentane. In H-ZSM-5, we find that the diffusivity of *n*-hexane in mixtures with its branched isomer is determined by two factors: (i) the interaction with acid sites, strong for the linear alkane, which decreases the diffusivity and (ii) the presence of 2-methylpentane which has an order of magnitude lower diffusivity. At low 2-methylpentane loadings the influence of the acid sites is dominating. However, at a loading of about 2.7 molecules per unit cell, the effect of pore blocking by the preferential location of the branched alkane in the intersections dominates. The diffusivities are then more or less equal in silicalite-1 and H-ZSM-5.

3.3 Self-diffusivity of *n*-Pentane and *n*-Hexane and their Mixtures in Silicalite-1

We have earlier studied the concentration dependence of the self-diffusivity of *n*-hexane in large crystals of silicalite-1 and H-ZSM-5 zeolites [81]. A rather peculiar monotonic increase in the diffusivity was observed with increasing alkane loading for both zeolites up to 4 molecules per unit cell. The diffusion coefficient in H-ZSM-5 was found to be approximately half of that in silicalite-1 due to the interaction of *n*-hexane with the Brønsted acid sites. The increase in the diffusivities with the loading was assumed to be caused by repulsive interactions between the molecules adsorbed in the channel intersections and

the adjacent straight channel. However, we should note that this explanation is rather speculative and has to be supported by theoretical investigations. Here, we will report similar investigations for *n*-pentane and mixtures of *n*-pentane and *n*-hexane. Before discussing in more detail the diffusivities of such mixtures for which PEP is a unique technique, we will focus on the self-diffusivity of *n*-pentane in silicalite-1 as a function of loading at various temperatures. At temperatures of 473 and 453 K the hydrocarbon loading is low, i.e., less than 1.5 molecules per unit cell making accurate determinations of self-diffusion coefficients difficult. At 433 K the loading corresponds to about 3.5 molecules per unit cell. At low temperatures (373 and 393 K) the diffusion coefficient of *n*-pentane increases with its loading. This is in line with previous results for *n*-hexane diffusion in silicalite-1 [81]. In that study, we reported the peculiar phenomenon that an increase of *n*-hexane loading from 0.1 to 4 molecules per unit cell led to a significant increase in self-diffusivity. This unexpected effect is tentatively explained by repulsive interactions between hydrocarbon molecules, leading to an increase in the jump rate between adjacent sites.

Such interactions and their effect on diffusivity have been described by Paschek and Krishna for isobutane in silicalite-1 [82]. We tentatively propose that the concentration dependence of *n*-pentane diffusivity reported here is due to similar effects. In short, this means that repulsive intermolecular interactions lead to increased mobility of *n*-pentane. This tallies with the absence of a siting preference for this hydrocarbon. One would expect slightly weaker repulsions for *n*-pentane compared to the longer *n*-hexane molecules, especially at high temperatures. Indeed, as only one molecule (*n*-pentane or *n*-hexane) fits into a channel or an intersection, the distance between the *n*-pentane molecules adsorbed in the straight channels and the intersections is larger than the corresponding distance for *n*-hexane molecules. One expects that repulsive forces decrease with an increase in the intermolecular distance. At high temperatures, these interactions are weaker as predicted by Paschek and Krishna [82]. This effect is also found in our experiments as the diffusivity of *n*-pentane does not increase with loading at high temperatures ($T > 493$ K).

Besides repulsive interactions between the molecules, other factors influence the diffusion of *n*-pentane in silicalite-1. Theoretical calculations [17–19, 53] have shown a decrease in the diffusivity with loading when repulsive interactions are not taken into account. In this case, pore occupancy plays a dominant role. As the loading increases, the probability for the molecule to jump to the neighboring adsorption site decreases since the chance that the site is already occupied increases. Hence, the molecule will reside longer at its current location. This effectively decreases the jump frequency and thus the self-diffusion coefficient. According to mean-field theory, diffusivity should be proportional to the fraction of the unoccupied sites [2]. For silicalite-1, self-diffusivity was shown to decrease slightly faster with the occupancy due to correlation effects [19]. Krishna and Paschek [84] determined

a jump diffusion at a given occupancy as a jump diffusion at zero occupancy proportional to the vacancy factor and to the repulsion factor, which in turn is also concentration dependent. Therefore, we assume that self-diffusion of *n*-pentane in silicalite is simultaneously affected by the hydrocarbon loading of the zeolite, that causes a decrease in the diffusion, and by repulsive interactions between the molecules, that cause an increase in their mobility. These two effects compete with each other. Experimental conditions determine which of these two dominates. For example, up to a certain partial pressure, molecules such as branched alkanes are preferentially adsorbed in the channel intersections [44, 82, 85]. Under these conditions, there is no repulsion between the molecules, and diffusion decreases with the loading. As soon as the molecules start to appear in the straight channels, diffusion increases [82]. To our opinion, the observation that at relatively high temperatures (433–473 K), the self-diffusion coefficient of *n*-pentane does not change with concentration (Fig. 17) indicates that the pore occupancy effect is compensated by the repulsive interactions between the molecules. At 433 K, the concentration of *n*-pentane in the micropores varied from 0.5 to 3.5 molecules per unit cell. At these pore occupancies, and making the assumption that other interactions are absent, a decrease in the diffusivity is predicted by Coppens et al. [19]. The deviant observation can be tentatively explained by inclusion of repulsive interactions that compensate this decrease of the molecular mobility. On the other hand, at high temperatures diffusion is faster

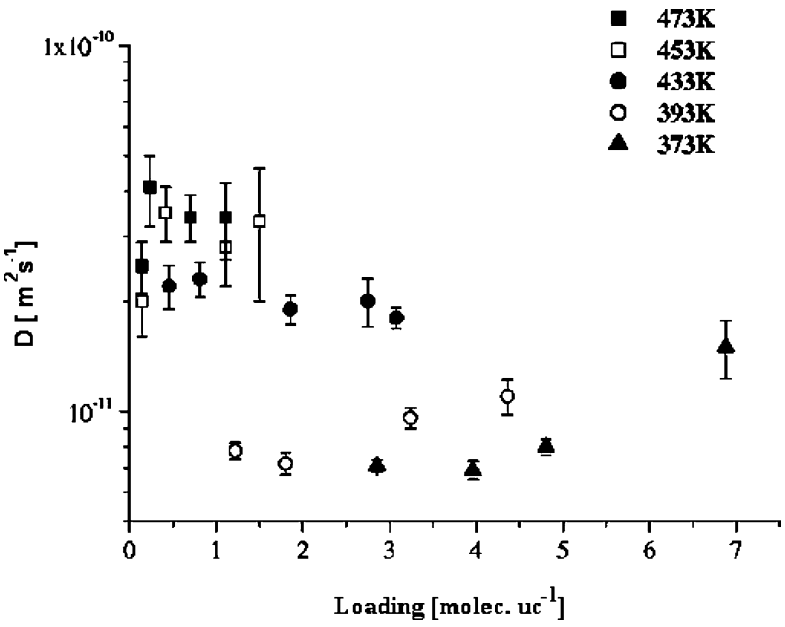

Fig. 17 Self-diffusivity of *n*-pentane in silicalite-1 at various temperatures and loadings

and the repulsive interactions should be weaker. Therefore, such interactions do not dominate over the pore occupancy effect and the diffusion coefficient does not change. At low loadings, both the occupancy and repulsion effects are apparently not of overriding importance, and we find almost constant values for the self-diffusion coefficient within the experimental accuracy limits. At lower temperatures (373–393 K), we observe that diffusion becomes faster at higher loadings. This is similar to our earlier report on *n*-hexane diffusivity [81] and is explained by the dominance of repulsive interactions.

In the work of Heink et al. [86] a decrease in the diffusivity of *n*-pentane in silicalite-1 up to loadings of 0.75 molecules per unit cell and higher than four molecules per unit cell was found with PFG NMR. Despite an apparent disagreement, we note that in their experiments at low concentrations the pore occupancy effect was dominating, resulting in a lowering of the jump frequency with loading. The absence of such an increase in the present study may lie in the lower experimental accuracy. At high loadings (4–12 molecules per unit cell), a decrease of *n*-pentane diffusion was measured [86, 87]. Probably, the occupancy effect is more dominant than the intermolecular repulsive effect in this range. On the other hand, it is known that the maximum sorption capacity of silicalite-1 for *n*-pentane is approximately eight molecules per unit cell, implying that at loadings higher than eight molecules per unit cell the diffusion coefficients do not pertain exclusively to micropore diffusion. Our interpretation is further supported by diffusion measurements of light alkanes in silicalite-1 performed by van de Graaf et al. [91] using a membrane permeation technique. At 303 K, an increase of the intracrystalline diffusivity was observed for C_1-C_3 alkanes. At higher temperatures, the diffusivity did not change with increasing concentration in line with our results. For *n*-propane, the diffusivity had a maximum at pore occupancy of approximately 0.8. Apparently, up to that occupancy diffusivity increases due to the stronger influence of the proposed repulsive interactions. At higher loadings the pore occupancy effect dominates resulting in a decrease of the diffusivity.

Summarizing, we propose the following for *n*-pentane diffusion in silicalite-1. At very low loadings, *n*-pentane diffusion coefficients are constant or slightly decrease with the total pore occupancy. This possible decrease is due to the pore occupancy effect but is too small to be detected by the TEX-PEP method. At intermediate loadings, molecules occupy both straight and zigzag channels and start to develop repulsive interactions. The expected decrease in diffusion coefficient with pore occupancy is compensated by an increase in the jump frequency due to such repulsive interactions. At high loadings, the repulsion effect is dominating and the self-diffusion coefficient increases. At even higher loadings, we expect the diffusion to slow down due to strong pore occupancy effects. Note that the repulsive interactions do not have a noticeable impact on the molecular mobility at high temperatures, and consequently the effect of loading on the diffusivity is small at high temperature. In this latter case it is not possible to work at higher loadings because the

Table 6 Comparison of *n*-pentane diffusivities reported in literature with those obtained by TEX-PEP

Method	$D \times 10^{-11}$ [$m^2\ s^{-1}$]	Conditions	Refs.
TEX-PEP	0.7–1.05	373 K, 2.9–7.1 molec.uc^{-1}	
Membrane technique	0.24	334 K, –	[88]
ZLC	0.2	334 K, –	[71, 72]
FR	40	303 K, 7 molec.uc^{-1}	[89]
PFG NMR	40	330 K, 4 molec.uc^{-1}	[86]
PFG NMR	204	334 K, 4–8 molec.uc^{-1}	[87]
SCM	1	300 K, 0.5 kPa	[90]
MD	98.5	333 K, 4 molec.uc^{-1}	[53]

adsorbate has a limited concentration at higher temperatures by the technical design of the feed system.

Table 6 shows a comparison between diffusion coefficients of *n*-pentane in silicalite-1 measured by various macro- and microscopic techniques as well as deduced from molecular dynamics simulations. However, we did not find reports where diffusion coefficients of *n*-pentane in silicalite-1 were measured under conditions similar to this study. TEX-PEP values are in a good agreement with values provided by macroscopic techniques such as the Membrane technique [88], ZLC [71, 72] and the SCM technique [90]. The diffusivity provided by the macroscopic frequency response method is an order of magnitude higher [89]. Tentatively, we explain this to the significantly lower temperature and higher loading which could lead to a dominating influence of the repulsive interactions. Usually, diffusivities measured by microscopic techniques (PFG NMR) or computer simulations are significantly higher than those from macroscopic methods. The authors of a novel macroscopic ultra-high vacuum technique, Multitrack [92], claimed that one of the reasons for the lower values of the diffusivities measured by macroscopic methods is the diffusion resistance caused by the presence of a carrier gas. Comparison with the data found in the literature shows that the diffusivities provided by the TEX-PEP method are in reasonably good agreement with the values supplied by other macroscopic techniques.

Activation Energy of *n*-Pentane Diffusion in Silicalite-1

We have tried to establish whether there is any influence of the proposed repulsive interactions on the apparent activation energy for diffusion. In a theoretical study on isobutane diffusion in silicalite-1 [82], a change in the apparent activation energy was determined. At lower temperatures, the apparent activation energy was lower than at elevated temperatures. This effect was proposed to be caused by repulsive interactions. We determined the ap-

Table 7 Apparent activation energy of diffusion for *n*-pentane in silicalite at various partial pressures

Pressure [kPa]	E_{app} [kJ mol^{-1}]
0.5	18 ± 4
1.0	27 ± 4
3.3	21 ± 3
9.0	13 ± 2

parent activation energy for diffusion of *n*-pentane in silicalite-1 at partial pressures of 0.5, 1.0, 3.3 and 9.0 kPa in the temperature interval 393–473 K. The results are collected in Table 7. At low hydrocarbon partial pressures the accuracy was low which is related to the lower accuracy in the determination of the self-diffusivities. Nevertheless, the values are in the range of literature data, varying from 8.3 kJ mol^{-1} (PFG NMR [86]) to 21 kJ mol^{-1} (FR, [89]). Evidently, the apparent activation energy does change with the partial pressure. We explain this by the competing influence of two factors, i.e., the pore occupancy and the repulsive interactions. Which of these two effects is dominant depends on the temperature and adsorbate concentration. The *n*-pentane loadings in silicalite-1 are depicted in Fig. 18.

Earlier, we have reported that the apparent activation energy for diffusion of 3-methylpentane in silicalite-1 increases with the partial pressure. This was explained by the pore occupancy effect influencing the pre-exponential fac-

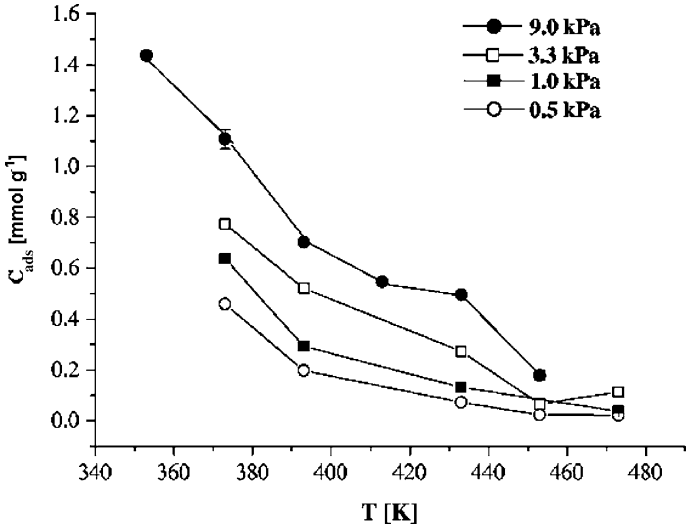

Fig. 18 *n*-Pentane loadings at various temperatures and partial pressures in silicalite-1

tor of diffusion which is proportional to the jump frequency, D_{inf}. This is explained by the fact that under fixed partial pressure conditions the zeolite loading will vary as a function of temperature.

On the other hand, the apparent activation energy for *n*-pentane diffusion in silicalite-1 might decrease due to the repulsive interactions as shown earlier. The lower apparent activation energy at a partial pressure of 0.5 kPa is due to the compensation of the pore occupancy and repulsive effects. We speculate that the apparent activation energy is close to the one at zero loading. At higher partial pressures the pore occupancy starts to play a more significant role, leading to an increase in the apparent activation energy. At high partial pressure (9.0 kPa), the apparent activation energy has the lowest value, which is attributed to the strong increase in diffusivity due to the dominating repulsive interactions.

The current trends identified for *n*-pentane are strikingly similar to those for *n*-hexane. TEX-PEP provides the unique possibility to study diffusion of two linear hydrocarbon in two separate sets of experiments. In a first set, *n*-pentane is labeled and its diffusion coefficients are determined in a mixture with non-labeled *n*-hexane, while the reverse is done in a second set. The experiments have been performed at a temperature of 433 K and the total hydrocarbon pressure was kept constant at 6.6 kPa by varying the ratio between *n*-hexane and *n*-pentane in the gas phase. Figure 19 shows the loadings of both components in the mixture as a function of the *n*-hexane fraction in

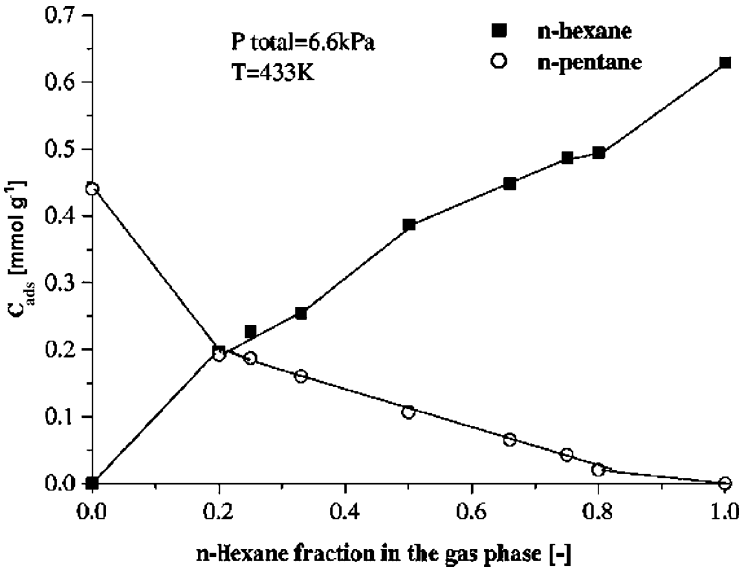

Fig. 19 Loadings of mixture components in silicalite as a function of *n*-hexane fraction in the gas phase (total hydrocarbon pressure 6.6 kPa, 433 K)

the gas phase. Obviously, *n*-hexane is preferentially adsorbed over *n*-pentane. In the equimolar gas mixture, the *n*-hexane loading was approximately three times higher compared to that of *n*-pentane (0.39 and 0.13 mmol g^{-1}, respectively). This corresponds to the larger heat of adsorption of *n*-hexane in silicalite-1 than that of *n*-pentane, 71 and 42 kJ mol^{-1} [93], respectively. Since both alkanes are likely to be situated throughout the micropore space [85] under the applied conditions, the stronger adsorption is due to enthalpic and not entropic reasons. Clearly, this corresponds to the higher single-component loading for *n*-hexane (0.63 mmol g^{-1}) than that for *n*-pentane (0.45 mmol g^{-1}).

Figure 20 shows the self-diffusivities of *n*-pentane and *n*-hexane as a function of gas mixture composition. The loadings of both components depend on the gas phase composition fraction. Note that in these experiments the total hydrocarbon pressure is kept constant (6.6 kPa). The loading of a feed of pure *n*-hexane under these conditions (433 K, 6.6 kPa) is 3.6 molecules per unit cell. Unexpectedly, we observe a lower diffusion coefficient for pure *n*-pentane than for *n*-pentane in a mixture with *n*-hexane. Tentatively, we ascribe this to the more drastic increase in *n*-hexane diffusivity with loading than for *n*-pentane. As discussed earlier, this can be ascribed to stronger repulsive interactions for the longer hexane hydrocarbons. It is clear from Fig. 20 that at low *n*-hexane concentrations, its diffusion is slower than of *n*-pentane. The diffusivity of hexane increases with *n*-hexane loading, while the diffusivity of pure *n*-pentane was found to be independent on the concentration at this temperature. Repulsion between *n*-pentane

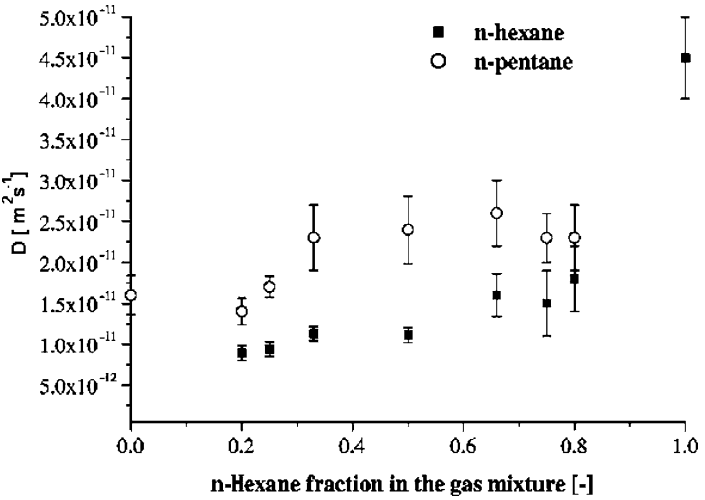

Fig. 20 Self-diffusivities of mixture components in silicalite at various gas mixture compositions (total hydrocarbon pressure 6.6 kPa, 433 K). Gas mixture composition is determined by the ratios between the components in the gas phase

molecules should be weaker than between *n*-hexane molecules. In mixtures, *n*-pentane and *n*-hexane molecules are randomly distributed in the zeolite. We argue that also repulsive interactions are present between *n*-pentane/*n*-hexane molecules. In our crude estimation, the distance between *n*-hexane/*n*-pentane is shorter than that between npentane/*n*-pentane molecules. Thus, increasing the *n*-hexane loading effectively replaces neighboring *n*-pentane by *n*-hexane molecules. This leads to stronger intermolecular repulsive interactions and a consequent increase in the self-diffusion coefficient of the shorter alkane. From Fig. 20, it is clear that *n*-hexane diffusion in mixtures with *n*-pentane is slower compared to its single-component diffusion. Our simple model can explain this by a decrease of intermolecular repulsive interactions in the order of *n*-hexane/*n*-hexane > *n*-hexane/*n*-pentane > *n*-pentane/*n*-pentane. This also indicates that in the absence of such interactions *n*-hexane is slower than *n*-pentane, which is a reasonable behavior to expect. As the concentration of *n*-hexane in the silicalite pores increases further, diffusion of *n*-hexane slightly increases due to increased repulsions.

At first sight, these results are somewhat different from those obtained by Masuda et al. [55] for *n*-heptane/*n*-octane mixtures in silicalite-1. A decrease in the diffusivity of the faster-diffusing *n*-heptane was observed as the loading of slower *n*-octane increased, while the octane diffusivity did not change in the presence of *n*-heptane. This difference may be attributed to different experimental conditions, since the temperature was higher (448–498 K) and the total pressure significantly lower (13 Pa). In this case, a relatively small pore occupancy is expected and repulsive interactions should be minimal. This leads to similarly low mobility of the faster hydrocarbon as of the slow one.

In conclusion, TEX-PEP allowed us to study the concentration dependence of self-diffusion of *n*-pentane and its diffusion in mixtures with *n*-hexane in silicalite-1. Diffusion of *n*-pentane was found to be independent on the loading at high temperatures, while at lower temperatures a slow increase in the self-diffusion coefficient was observed. In a tentative simple model, we attribute this to intermolecular repulsive interactions between the molecules located in the intersections of the straight and zigzag channels and those sited in the adjacent straight channels. This may result in an increase in the hydrocarbon mobility of the molecules [82]. However, *n*-pentane diffusivity is also affected by the pore occupancy, which causes a decrease in the diffusivity. Although these two factors are competing, it appears that they more or less compensate each other at high temperatures. As a result diffusion is independent of the concentration. At low temperatures, repulsive interactions are stronger, and the diffusivity tends to increase with increasing loading. The complex effects also influence the apparent activation energy for diffusion.

In mixtures with *n*-hexane for which the influence of intermolecular repulsive forces appear to be stronger, we find that *n*-pentane diffusivity is enhanced. This is most likely due to higher repulsive forces between *n*-pentane/*n*-hexane molecules residing in adjacent pore positions than between

n-pentane/*n*-pentane pairs. Thus, at high loading of *n*-hexane, the mobility of *n*-pentane molecules becomes very close to that of *n*-hexane. Molecularly, this can be interpreted that the diffusivity of the shorter alkane is totally determined by the longer one. On the contrary, *n*-hexane diffuses slower in mixtures with *n*-pentane compared to pure *n*-hexane under similar conditions. With increasing fraction of *n*-pentane the repulsive forces become weaker and the diffusivity of *n*-hexane becomes even slower than that of *n*-pentane. It appears that the presence of another hydrocarbon with a slightly different diffusion coefficient results in a complex behavior depending on the temperature and the total and fractional micropore occupancy. These experimental data cannot yet be described by molecular models in detail and call for further refinement of molecular simulations. A crucial point will be to develop methods to determine self-diffusion coefficients at realistic hydrocarbon loadings.

4 Conclusions

Zeolites are widely used in the petrochemical industry as catalysts and adsorbents. In order to enhance the understanding of the complex interplay of reaction and diffusion, there is a large interest in understanding of diffusion processes of alkanes in medium-pore zeolites. Much attention has been paid to study diffusivity of alkanes in MFI zeolite, mostly of the all-silica type (silicalite-1). In the present contribution, we have studied single-component self-diffusion coefficients of hexanes in silicalite-1 and its acidic counterpart, H-ZSM-5 by tracer exchange positron emission profiling (TEX-PEP). Moreover, we investigated the diffusivity of mixtures of alkanes. For the first time, the diffusion of *n*-pentane and *n*-hexane in mixtures was studied in detail. This shows that positron emission profiling is a powerful technique for in situ investigations of the adsorption and diffusive properties of hydrocarbons in zeolites. As the technique is based on the labeling of a small portion of the hydrocarbons, one can perform tracer exchange experiments under chemical steady-state conditions. This allows one to extract self-diffusion coefficients of hydrocarbons at finite loadings, even in the presence of another unlabeled alkane.

We have discussed the adsorption and diffusion of binary mixtures of linear (*n*-hexane) and branched (2-methylpentane) alkanes in silicalite-1. It turned out that not only the size but also the siting of the molecules in the particular zeolite plays an important role in the behavior of the mixture components. A slight preference for the adsorption of *n*-hexane over 2-methylpentane was observed because of the higher packing efficiency of the linear alkane. This is due to the preferential location of the branched alkane in the zeolite intersections. A consequence of this is that the diffusivity of *n*-hexane

is strongly influenced by that of the slower branched component. A drastic decrease in the diffusivity of *n*-hexane is observed at a 2-methylpentane loading of about 2.75 molecules per unit cell. This is explained by blocking of the channel intersections. The loading roughly corresponds to the situation where three out of four channel intersections are occupied by the isohexane.

A comparison between silicalite-1 and H-ZSM-5 teaches that acid sites have a profound influence on the self-diffusivity of alkanes. The self-diffusivities of both components decrease strongly, and we observe a significant preferential adsorption of the linear over the branched hexane. This is caused by the relatively stronger interaction of the linear hexane with the acid sites. On the contrary, 2-methylpentane loadings in mixtures in silicalite-1 and H-ZSM-5 are very close. In H-ZSM-5, the diffusivity of the linear alkane in mixtures with the branched alkane is influenced by two factors (i) interaction with the acid sites, which decreases the diffusivity by approximately a factor of two and (ii) the presence of 2-methylpentane, which has a ten-times lower diffusivity. At low loadings of the branched alkane, the interactions with the acid sites is prevailing. As soon as the loading of isohexane exceeds approximately 2.7 molecules per unit cell, the effect of the Brønsted sites on the diffusion becomes negligible compared to the blockage of the pore network connection by the branched alkane.

Our earlier studies confirmed that diffusion of 3-methylpentane in silicalite-1 decreases with increasing loadings. This simple behavior points to the absence of intermolecular interactions, which tallies with the notion that this branched alkane is preferentially located in the zeolite's intersections. Similar measurements with *n*-hexane showed that its self-diffusivity increases with increasing loading. This is tentatively attributed to intermolecular repulsive interactions which are more pronounced between *n*-hexane molecules located in the intersections and the channels. Here, we investigated the diffusivity of *n*-pentane as a single component and in mixtures with *n*-hexane in silicalite-1. From the single-component *n*-pentane measurements, we derived that the increase of diffusivity with loading was less dramatic than for *n*-hexane. This is in line with the smaller dimensions of the C_5 alkane which should reduce the repulsive interactions. Interestingly, we found that *n*-pentane diffuses faster in a mixture with *n*-hexane than in a single-component experiment at the same total hydrocarbons partial pressure. This is believed to be caused by stronger repulsive interactions with *n*-hexane than between *n*-pentane molecules. Consequently, we can explain that at high loadings of *n*-hexane, the mobility of *n*-pentane molecules becomes very close to that of *n*-hexane. On the contrary, *n*-hexane diffuses slower in mixtures with *n*-pentane compared to the single-component diffusivity under similar conditions. Upon increasing the fraction of *n*-pentane, repulsive interactions become weaker and the diffusivity of *n*-hexane becomes even slower than that of *n*-pentane.

Summarizing, the diffusion of hydrocarbon molecules in medium-pore zeolites is determined by a complex interplay of factors, such as the loading,

the temperature, the preference for certain pore locations, the interactions with other hydrocarbons of the same type or others and the presence of acid protons. In diffusion of mixtures, pore blockage by one of the components might occur, thus strongly decreasing the diffusivity of the fast hydrocarbon.

References

1. Baerlocher C, Meier WM, Olson DH (2001) Atlas of zeolite framework types, 5th ed. Elsevier, Amsterdam, The Netherlands
2. Jost W (1960) Diffusion in solids, liquids and gases. Academic Press, New York
3. Kärger J, Ruthven DM (1992) Diffusion in zeolites and other microporous solids. John Wiley & Sons, Inc, New York
4. Chen NY, Degnan TF Jr, Smith CM (1994) Molecular transport and reaction in zeolites design and application of shape selective catalysis. VCH Publishers, New York
5. Benes NE, Verweij H (1999) Langmuir 15:8292
6. Kauzmann W (1966) Kinetic theory of gases. Addison-Wesley, Reading
7. Post MFM (1991) In: Van Bekkum H, Flanigen EM, Jansen JC (eds) Introduction to zeolite science and practice. Elsevier, Amsterdam, pp 391–443
8. Post MFM (1991) Stud Surf Sci Catal 58:391
9. Wakao N, Kaguei S (1982) Heat and mass transfer in packed beds. Gordon and Breach Science, London
10. Weisz PB (1973) Chem Tech 3:498
11. Fick A (1855) Ann Phys 94:59
12. Barrer RM, Jost W (1949) Trans Faraday Soc 45:928
13. Einstein A (1905) Ann Phys 17:549
14. Paschek D, Krishna R (2001) Chem Phys Lett 333:278
15. Skoulidas AI, Sholl DS (2001) J Phys Chem B 105:3151
16. Barrer RM (1941) Trans Faraday Soc 37:590
17. Theodorou DN, Wei J (1983) J Catal 83:205
18. Tsikoyiannis J, Wei J (1991) Chem Eng Sci 46:233
19. Coppens MO, Bell AT, Chakraborty AK (1998) Chem Eng Sci 53:2053
20. Kärger J, Pfeifer H (1987) Zeolites 7:90
21. Xiao J, Wei J (1992) Chem Eng Sci 47:1123
22. Riekert L (1970) Adv Catal 21:281
23. Koriabkina AO, De Jong AM, Schuring D, Van Santen RA (2002) J Phys Chem B 106:9559
24. Haynes HW, Sarma PN (1973) AIChE J 19:1043
25. Noordhoek NJ, Van Ijzendoorn NJ, Anderson BG, De Gauw FJ, Van Santen RA, De Voigt MJA (1998) Ind Eng Chem Res 37:825
26. Mangnus AVG (2000) A detection system for Positron Emission Profiling, Ph.D. thesis. Eindhoven University of Technology, Eindhoven, The Netherlands
27. Ferrieri RA, Wolf AP (1984) J Phys Chem 88:2256
28. Ferrieri RA, Wolf AP (1984) J Phys Chem 88:5456
29. Baltensperger U, Ammann M, Bochert UK, Eichler B, Gäggeler HW, Jost DT, Kovacs JA, Türler A, Sherer UW, Baiker A (1993) J Phys Chem 97:12325
30. Hawkesworth MR, Parker DJ, Fowles P, Crilly JF, Jefferies NL, Jonkers G (1991) Nucl Instrum Methods A310:423
31. Hensel F (1996) Institut Sicherheitsforschung, Forschungszentrum Rossendorf, Dresden D-01314, Germany. FZR, FZR-152, p 12

32. Jonkers G, Vonkeman KA, Van der Wal SWA, Van Santen RA (1992) Nature 355:63
33. Jonkers G, Vonkeman KA, Van der Waal SWA (1993) In: Weijnen MPC, Drinkenburg AAH (eds) Precision Process Technology. Kluwer Academic Publishers, The Netherlands, p 533
34. Mangnus AVG, Van Ijzendoorn LJ, De Goeij JJM, Cunningham RH, Van Santen RA, De Voigt MJA (1995) Nucl Instrum Methods B99:649
35. Schumacher RR, Anderson BG, Noordhoek NJ, De Gauw FJMM, De Jong AM, De Voigt MJA, Van Santen RA (2001) Microporous Mesoporous Mater 35–36:315
36. Noordhoek NJ, Schuring D, De Gauw FJMM, Anderson BG, De Jong AM, De Voigt MJA, Van Santen RA (2002) Ind Eng Chem Res 41:1973
37. Cunningham RH, Mangnus AVG, Van Grondelle J, Van Santen RA (1996) J Mol Catal A 107:153
38. Rosen JB (1952) J Chem Phys 20:387
39. Nijhuis TA, Van den Broeke LJP, Linders MJG, Van de Graaf JM, Kapteijn F, Makkee M, Moulijn JA (1999) Chem Eng Sci 54:4423
40. Hong U, Kärger J, Kramer R, Pfeifer H, Seiffert G, Müller U, Unger KK, Lück HB, Ito T (1991) Zeolites 11:816
41. Schiesser WE (1991) The Numerical Method of Lines: Integration of Partial Differential Equations. Academic Press, San Diego
42. Marquardt D (1963) J Appl Math 11:431
43. Atkins PW, De Paula J (2002) Physical Chemistry, 7th ed. Oxford University Press, Oxford, United Kingdom, pp 822–824
44. Vlugt TJH, Krishna R, Smit B (1999) J Phys Chem B 103:1102
45. Zhu W, Kapteijn F, Moulijn JA (2001) Microporous Mesoporous Mater 47:157
46. June RL, Bell AT, Theodorou DN (1992) J Phys Chem B 96:1051
47. June RL, Bell AT, Theodorou DN (1990) J Phys Chem B 94:1508
48. Zhu W, Kapteijn F, Van der Linden B, Moulijn JA (2001) Phys Chem Chem Phys 3:1755
49. Calero S, Smit B, Krishna R (2001) J Catal 202:395
50. Schuring D, Koriabkina AO, De Jong AM, Smit B, Santen RA (2001) J Phys Chem B 105:7690
51. Breck DW (1974) Zeolite Molecular Sieves. John Wiley, New York
52. Snurr RQ, Kärger J (1997) J Phys Chem B 101:64
53. Schuring D, Jansen APJ, Van Santen RA (2000) J Phys Chem B 104:941
54. Jost S, Bar NK, Fritzsche S, Haberlandt R, Kärger J (1998) J Phys Chem B 102:6375
55. Masuda T, Fujikata Y, Ikeda H, Hashimoto K (2000) Microporous Mesoporous Mater 38:323
56. Gergidis LN, Theodorou DN (1999) J Phys Chem B 103:3380
57. Nivarthi SS, Davis HT, McCormick AV (1995) Chem Eng Sci 50:3217
58. Förste C, Germanus A, Kärger J, Pfeifer H, Caro J, Pilz W, Zikánová A (1987) J Chem Soc Faraday Trans 83:2301
59. Eder F (1996) Thermodynamics and siting of alkane sorption in molecular sieves, Ph.D.Thesis. University of Twente, The Netherlands
60. Wu P, Debebe A, Ma Y (1983) Zeolites 3:118
61. Anderson J, Foger K, Mole T, Rajadhyaksha R, Sanders J (1979) J Catal 58:114
62. Valyon J, Onyestyak G, Rees LVC (2000) In: Proc of 2nd Pac Basin Conf, p 482
63. Zikanova A, Bülow M, Schlodder H (1987) Zeolites 7:11
64. Shen D, Rees LVC (1991) Zeolites 11:666
65. Masuda T, Fujikata Y, Nishida T, Hashimoto K (1998) Microporous Mesoporous Mater 23:157

66. Jost S, Bar NK, Fritzshe S, Haberlandt R, Kärger J (1999) In: Treacy MMC, Marcus BK, Bisher ME, Higgins JB (eds) Proc 12th Int Zeolite Conf, Baltimore, USA, July 5–10, 1998. Materials Research Society, Warrendale PA, USA, p 149
67. Bülow M, Schodder H, Rees LVC, Caro J, Richards R (1986) In: Murakami Y, Iijima A, Ward JW (eds) New developments in zeolite science and technology; Proc. 7th Int Zeolite Conf, Tokyo, Japan, 1986. Elsevier, Amsterdam, pp 579–586
68. Bülow M, Schodder H, Rees LVC, Caro J, Richards R (1986) Stud Surf Sci Catal 28:579
69. Hashimoto K, Masuda T, Murakami N (1991) In: Jacobs PA, Jäger NI, Kubelkova L, Wichterlova B (eds) Zeolite Chemistry and Catalysis; Proc Int Symp, Prague, Czechoslovakia, September 8–13, 1991. Elsevier, Amsterdam, p 477
70. Hermann M, Niessen W, Karge HG (1996) In: LeVan MD (ed) Fundamentals of adsorption; Proc 5th Int Conf Fundamentals of adsorption, Asilomar Pacific Grove, California, USA, May 13–18, 1995. Kluwer Acad Publ Norwell, Mas, pp 377–384
71. Hermann M, Niessen W, Karge HG (1995) In: Beyer HK, Karge HG, Kiricsi I, Nagy JB (eds) Proc Int Symp Catalysis by Microporous Materials, Elsevier, Amsterdam, pp 131–138
72. Hermann M, Niessen W, Karge HG (1995) Stud Surf Sci Catal 94:131
73. Van-Den-Begin N, Rees LVC, Caro J, Bülow M (1989) Zeolites 9:287
74. Eic M, Ruthven DM (1989) In: Jacobs PA, Van Santen RA (eds) Zeolites: Facts, figures, future; Proc. 8th Int Zeolite Conf, Amsterdam, The Netherlands, 1989. Elsevier, Amsterdam, p 897
75. Eic M, Ruthven DM (1989) Stud Surf Sci Catal 49:897
76. Millot B, Methivier A, Jobic H, Moueddeb H, Dalmon JA (2000) Microporous Mesoporous Mater 38:85
77. Cavalcante CL, Ruthven DM (1995) Ind Eng Chem Res 34:185
78. Xiao J, Wei J (1992) Chem Eng Sci 47:1143
79. Keipert OP, Baerns M (1998) Chem Eng Sci 53:3623
80. Coppens MO, Bell AT, Chakraborty AK (1999) Chem Eng Sci 54:3455
81. Koriabkina AO, De Jong AM, Hensen EJM, Van Santen RA (2004) Microporous Mesoporous Mat 77:119
82. Paschek D, Krishna R (2001) Chem Phys Lett 342:148
83. Trout BL, Chakraborty AK, Bell AT (1997) Chem Eng Sci 52:2265
84. Krishna R, Paschek D (2002) Chem Eng J 85:715
85. Smit B, Maesen T (1995) Nature 374:42
86. Heink W, Kärger J, Pfeifer H, Datema KP, Nowak AK (1992) J Chem Soc Faraday Trans 88:3505
87. Datema KP, Den Ouden CJJ, Ylstra WD, Kuipers HPCE, Post MFM, Kärger J (1991) J Chem Soc Faraday Trans 87:1935
88. Hayhurst DT, Paravar A (1988) Zeolites 8:27
89. Song L, Rees LVC (1999) In: Treacy MMC, Marcus BK, Bisher ME, Higgins JB (eds) Proc 12th Int Zeolite Conf, Baltimore, USA, July 5–10, 1998. Materials Research Society, Warrendale PA, USA, p 67
90. Talu O, Sun MS, Shah DB (1998) AIChE J 44:681
91. Van de Graaf JM, Kapteijn F, Moulijn JA (2000) Microporous Mesoporous Mater 35–36:267
92. Nijhuis TA, Van den Broeke LJP, Van de Graaf JM, Kapteijn F, Makkee M, Moulijn JA (1997) Chem Eng Sci 52:3401
93. Sun MS, Talu O, Shah DB (1996) J Phys Chem B 100:17276